An application of numerical Fluid-Structure Interaction

on a local wave impacting a membrane LNG tank

Jochem Nonhebel

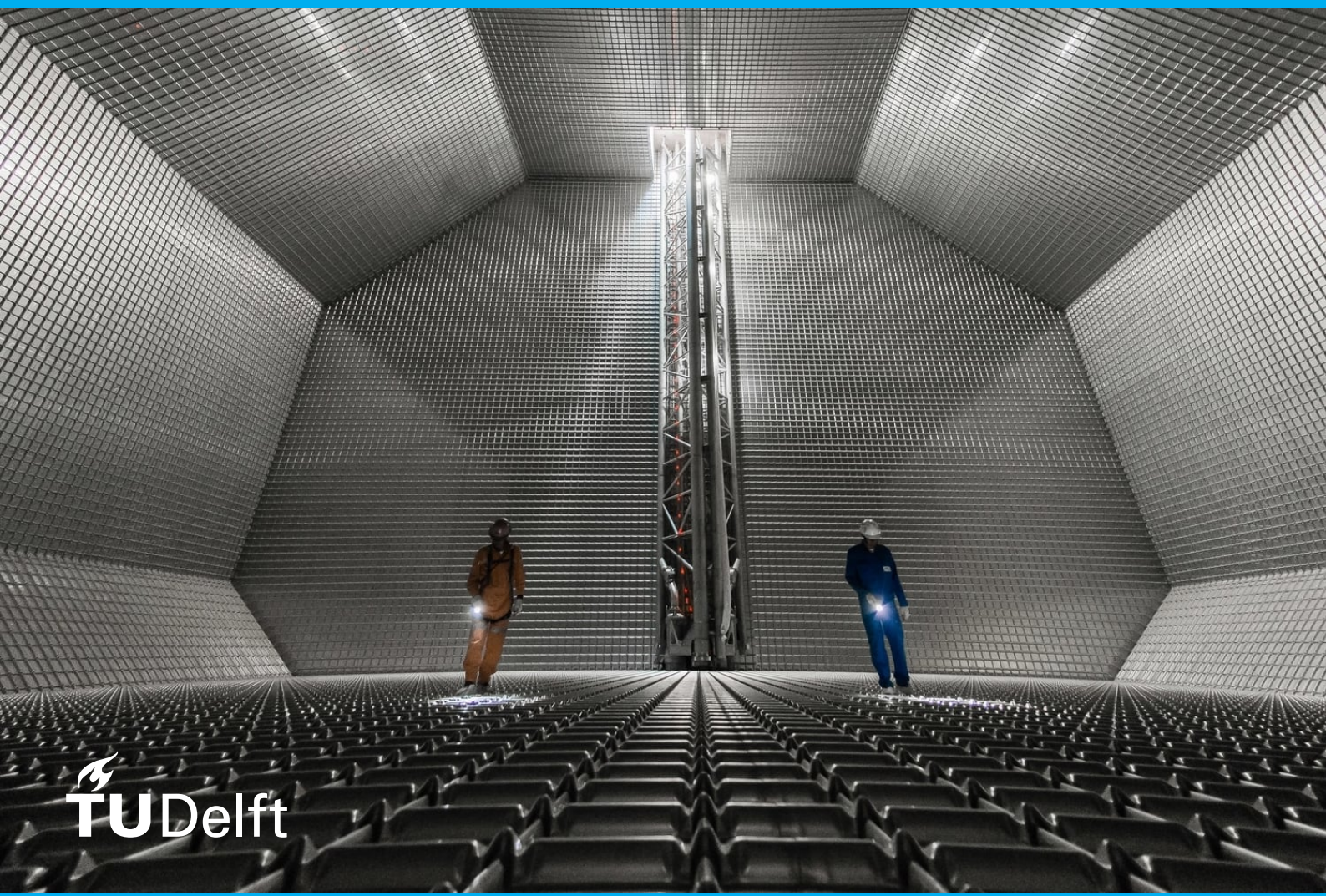

TU Delft

An application of numerical Fluid-Structure Interaction

on a local wave impacting a membrane LNG tank

by

Jochem Nonhebel

to obtain the degree of Master of Science

at the Delft University of Technology,

to be defended publicly on Thurseday April 11, 2019 at 5:00 PM.

Student number:	4157044	
Project duration:	July 4, 2018 – April 11, 2019	
Thesis committee:	Prof. dr. ir. M. L. Kaminski,	TU Delft, chairperson
	Ir. R. W. Bos,	TU Delft, daily supervisor
	Dr. ir. S.A. Miedema,	TU Delft

An electronic version of this thesis is available at http://repository.tudelft.nl/.

TU Delft ClassNK

Preface

The work to be described in this thesis is the final work to obtain the degree of Master of Science. The work has been performed partly in ClassNK, Tokyo and partly at the TU Delft. The work is part of the SLING project that focuses on understanding the sloshing behaviour of LNG in membrane tanks. Simulations in this work are performed with LS Dyna.

The process of writing this was great in the sense that not only a report with conclusions is the result, also a number of great professionals and friends I became stronger related to. And they should be thanked.

Professor Kaminski, for introducing me to his network of professionals, taking great, and personal, care during the process and providing trust.

Professor Poelma for providing the PIV results

Dr. T. Zhu and Dr. Matsumoto for opening the doors to ClassNK, in which I not only was provided with the best facilities that were required to do my work, but also providing me support and inspiration. Thank you Muneyuki Kokudai, Rei Miratsu and Keishi Shimizu for providing me with feedback, making me comfortable in Tokyo, learning me the Japanese culture and language.

The best coaches have the hardest times, not taking the work themselves, but taking the longer road and teaching their skills to their students. Thank you Reinier. For being personally involved and teaching me a great amount engineering and academic skills and supporting me all the way trough the process.

Time to time I realised that becoming successful can not be achieved without friends. I would like to thank Rixt, Hugo, Martin, Lianne, Maurtis, Tom and Wies. For their beneficial contribution to my thesis.

Jochem Nonhebel
Delft, April 2019

Summary

Natural gas accounts for just under a quarter of global energy demand. The gas is mainly delivered through pipelines, but is increasingly shipped overseas by liquefying it to LNG at -162 degrees Celcius.

Fluids, containing free surfaces inside ships are likely to start sloshing, as ships move on waves. These fluids induce impact loading on the walls of the tanks. These impacts induce amplified motions in the tanks membranes in the order of millimeters to centimeters, resulting in permanent deformation that could exceed acceptable risk levels.

In the industry one case of plastic deformation in the corrugated membranes of the LNG tanks was observed (Gavory and de Seze, 2009), but leakage was prevented. A growing desire for understanding sloshing behaviour raised and action was taken under the name of SLOHEL a JIP. Full scale experiments have been carried out. For investigating detailed structural response on *the effect of Fluid-Structure Interaction on a prediction of the plastic deformation of a Mark III membrane, subjected to a local wave impact*, a numerical application was carried out.

In this thesis, the experiments became input for a numerical Fluid-Structure Interaction model, that is strong two-way coupled. The structural response of a local wave impact is analysed using LS Dyna. Two-way|coupled and one-way|uncoupled results are compared. The pressures of the fluid model have been validated after making simplifications and are within a range of ±10% compared to measured results of the SLOSHEL experiments for an wave impact velocity of 7 m/s.

In the simulations three high pressure stages are identified on an impact between two corrugations. First, initial impact. Thereafter, lower corrugation impact ending with upper corrugation impact. At stage 3 large deformations were found in the foam layer behind the stainless steel membrane and for higher impact velocities also in the corrugated membrane.

Uncoupled simulations, in which the structure is considered as rigid for the fluid solver, but is able to respond flexible in the structural solver, were performed. In coupled simulations, a full interactive model is considered in which pressures update as a result of structural displacements. This results in dry frequencies for uncoupled simulations and wet frequencies for coupled simulations.

It was found that pressures in uncoupled simulations are in often higher. Displacements in the foam show for all cases higher displacements (10-25%) for uncoupled simulations. The plastic strains in the corrugated membrane are higher for high impact velocities (50-100%) for uncoupled simulations.

The significance of accounting coupled Fluid-Structure Interaction increases when deformations become non-linear. For this specific case, when yield stress of the corrugations in the membrane is exceeded id est when plastic strain occurs, uncoupled simulations are not able to obtain accurate predictions in structural response.

Nomenclature

Acronyms

CO_2	Carbon dioxide
ALE	Arbitrairy Lagrangian Eulerian
CCS	Cargo Containment System
CFD	Computational Fluid Dynamics
ELP	Elementary Loading Proces
FEM	Finite ELement Method
FSI	Fluid Structure Interaction
FVM	Finite Volume Method
iCFD	incompressible Computational Fluid Dynamics
LNG	Liquified Natural Gas
NG	Natural Gas
NOx	Nitrogen Oxides
SPH	Smoothed Particle Hydrodynamics

Contents

1

Introduction

The necessity to reduce greenhouse gasses increases strongly [28]. Devastating natural behaviour has shown to be result of climate change. Green house gases have shown to be a major factor in climate change, where human kind has contributed to increasing levels of greenhouse gases such as SOx, NOx and COx. Reduction of the human contribution of greenhouse gases is seen as necessary [29].

Although, great improvements on sustainable energy sources have been made in the last decades and very low polluting alternatives are economical available (solar-, wind energy), these sources of energy do not provide enough energy today and do not fit on any application. Today's energy demand is full filled for nearly a quarter by Natural Gas.

Natural Gas, as carrier of energy, exhaust 20% less CO2, 40 % less NOx and close to zero SOx compared to compared to conventional used bunker oil in shipping industry. Besides it is economically competitive. Transport of this gas on large scale is done by pipes and ships. Transport overseas shows an increasingly behaviour: 4% of the total natural gas demand in 1990 [1] and 9.8 % in 2016 [2].

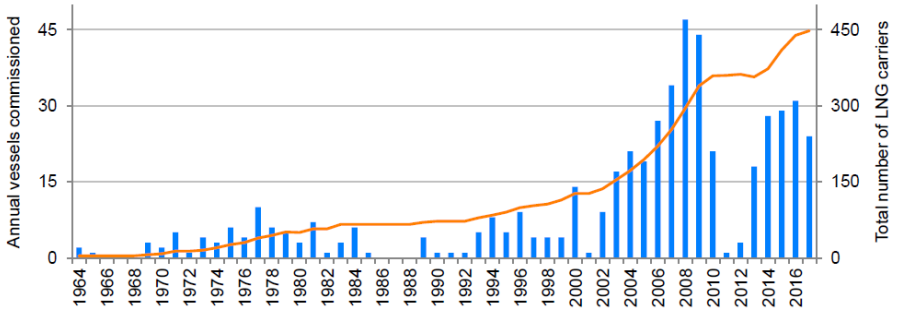

Figure 1.1: Global LNG carrier fleet. [2]

This thesis will focus on the tanks that are used inside ships that are used to transport LNG, named Cargo Containment Systems (CCS). The number of ships show increasing behaviour as can be seen in Figure 1.1 and in 2017, 478 vessels were operating in the market. Cooling the Natural Gas down to -163°C, makes the product Liquefied Natural Gas (LNG) and makes tanks able to carry 600 times more LNG than is was in gas phase.

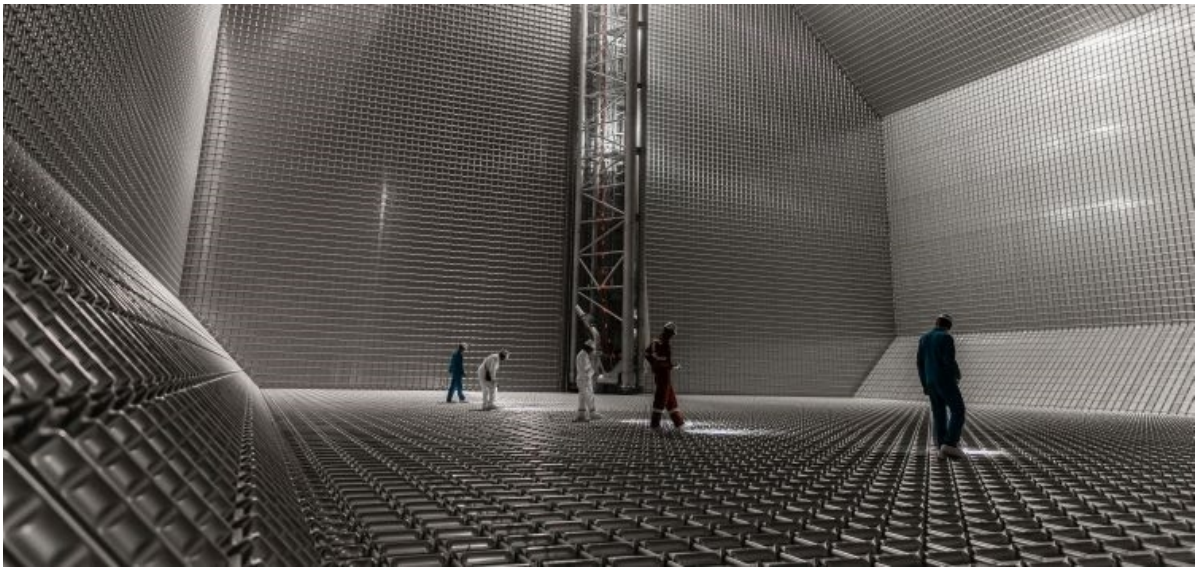

Figure 1.2: Mark III membrane tank technology. Courtesy GTT

Carrying this cryogenic [1] liquid requires structural support and strong isolation to control the temperature from the CCS. Unavoidable ships on oceans will move on waves, causing the liquid inside the CCS to move evidently. This effect is called sloshing.

Gaztransport & Technigaz (GTT) developed a solution under the name Mark III. This product contains stainless steel plates that contain corrugations, becoming a membrane looking tank (see Figure 1.2). The function of the corrugations is to withstand the forces that are induced due to the shrinking of the steel as a result of thermal contraction, or thermal strain.

As a response from the industry some damages were observed in the past. This was the driving force for GTT to performs research with the aim to improve the Mark III corrugation system. To enforce this research capacity, partners from industry and academic field joined the research under the the name Sloshel Joint Industry Project (JIP), leaded by MARIN, the Netherlands.

The research method included 1. Observation and measurement of ship motions. These motions are transformed to coupled motions and time traces, which makes it possible to use the data as input for laboratory research. 2. Than these motions are input for sloshing simulations. From these sloshing simulations pressure distributions are obtained. Also different free surface fluid was observed. This date could be used as input for a new set of experiments 3. From which 1:6 and full scale experiments were performed in the Netherlands by [22].

Interesting results of these experiments opened doors to the next research project. The current research is named under SLING (Slosing of Liquified Natural Gas), from which a large number of industry, academic and classification society partners are connected to this research group. The research is now leaded by the TU Delft in cooperation with MARIN. The aim of this research is to optimize the designs for tanks that are neither empty (<10%) nor full (<90%) filled as was only applied for long times, but that are partially filled. Optimisation is performed in terms of cost efficiency and acceptance of risk levels.

[1] the science of extreme cold materials

1.1. Mark III Containment System

The corrugated steel membrane is the first layer of 6 that prevents leakage from the CCS (see Figure 1.3). The following layer is a plywood layer followed by polyurethane foam. The function of the plywood layer is to distribute incoming pressure loads. The foam initially isolates the tank, maintaining the temperature. But, also it damps the pressures that are a result of sloshing loading. In which this foam has the function of isolating the tanks. Since these tanks are installed on ships that are exposes to severe conditions (waves, wind). Motion of the vessel induces motion of the LNG inside the tanks. And here the study area of Sloshing has born. Which makes the foam having a double function, namely making the structure strong enough to withstand sloshing loads.

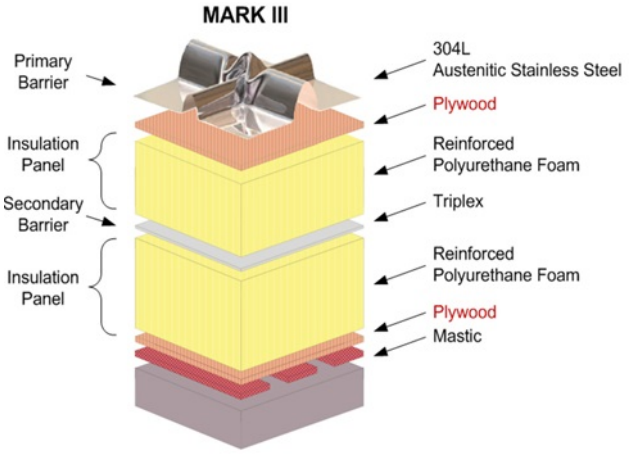

Figure 1.3: Layers of the Mark III LNG tanks. Courtesy GTT

Sloshing loads have shown in the past to be strong enough to plastic deform the corrugations. Modifications on the membrane have been made, that increases the strength of the structure. Enforcing the corrugations by forming additional ribs and supporting them by plywood beams below the corrugations has shown to make the corrugations less vulnerable.

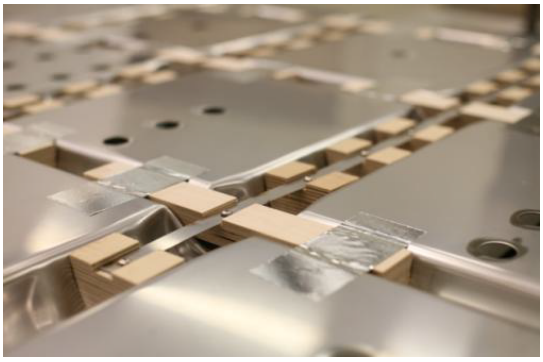

(a) Wooden wedges applied as reinforcement [12]

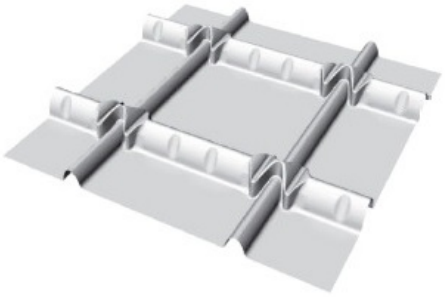

(b) Ribs added to the large corrugations [23]

Figure 1.4: Enforcement on the corrugations

1.2. Study on sloshing behaviour and structural response

Extensive amounts of physical experiments have been performed on fluid behavior as well as on the structural response.

One of the early methods of investigating sloshing behaviour and it's impacts was invented by [17]. The probability distribution of the sloshing impact loads and structural capacity of the CCS are derived and compared in order to define the probability of failure. The probability distribution of the sloshing impact loads are determined by sloshing model experiments. The experiments are performed on a 1:40 model, that is located on a hexapod (see Figure 1.5). The motions of the hexapod mimic the motions of LNG carriers. The scaled CCS' are supplied with numerous of pressure sensors.

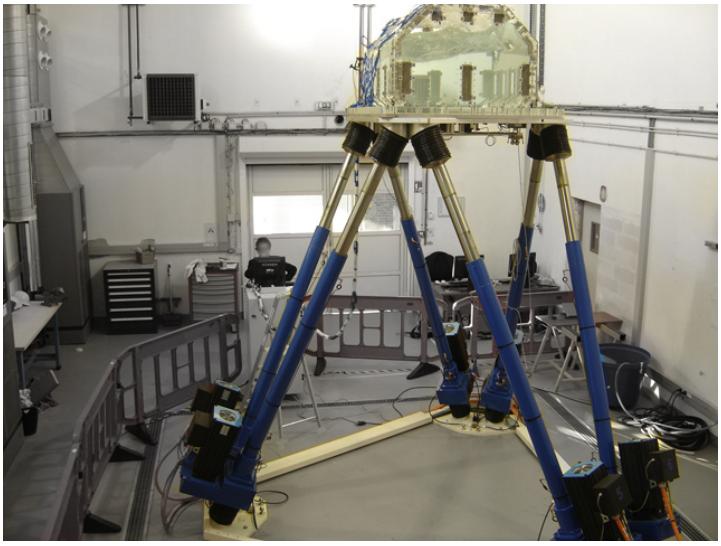

Figure 1.5: Model experiments 1:40 used to obtain pressure distributions. The Hexapod mimics ship motions. Courtesy GTT

Behaviour of the fluid has been studied on small scale. Wave shapes and and wave velocities are measured. This leaded to the next opportunity to use wave shapes and velocities as input for a new kind of experiments on full scale. These full scale experiments were performed [22] at MARIN in the Scheldt Delta flume (see Figure 1.6a. The outdoor facility is 240m long, 5m wide and 7m deep. The Mark III corrugations were installed at the end of the tank and the waves were created with a wave maker that applied a wave focusing technique. More information can be found in [12].

(a) Wave Flume

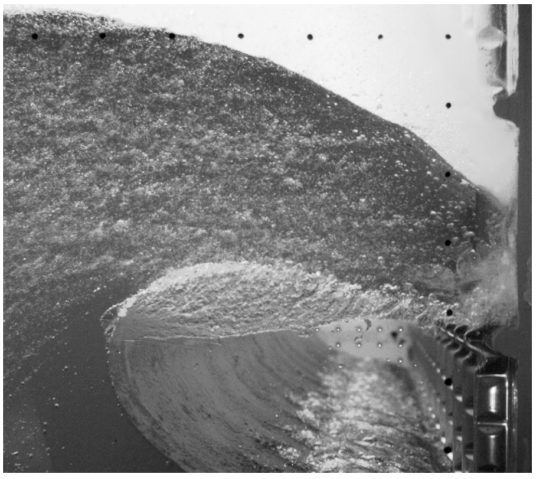

(b) Just before wave impact from the side.

Figure 1.6: Wave impact at the Flume Deltares 2010 [20]

Different experiments have been performed to study the structural resistance of many differ-

ent load cases. The study of Kim et. al [23] shows physical experiments on the corrugations where symmetric and asymmetric forces plastic deform the corrugations.

Besides, numerous of analytical and numerical models have been designed on both fluid-behaviour and structural response. Experimental work has been performed by [8]

It was found that when an extreme loading case due to a wave in a flume tank, the insulation foam deflects about 2.6mm in normal direction (see Figure 1.7a). Consequently the the initial shape of the corrugation is changed in several load cases. In this same test plastic deformation of the corrugation was found to be 5mm (see Figure 1.7b)

(a) Deformation of the foam (b) Deformed corrugation

Figure 1.7: Structural responses of the Foam and Corrugation due to a high impact [12]

In the development of corrugations in the past additional to the geometry, ribs were added in the large corrugations Figure 1.4. Anyway, Kim et. al [23] shows by physical experiments that ribs increase the amount of local stress in the material.

Temperatures in the CCS are, when loaded with LNG, around -163°C. This not only induces different material properties of the stainless steel, but also thermal strain occurs due to contraction of the steel. Therefore, in industry tanks will not completely made empty when unloading the tanks to reduce the cyclic loading induced by thermal strain.

Measured from [18], it was found that for 1:6 models vertical forces of 203N were measured on a small corrugation. It was found by [12] that highest force measured in a full scale loading case was 25.6kN on small corrugations where the transient pressure was measured 55.5bar.

So far numerous of numerical studies have been performed on the knot area and the corrugations area. These studies are all based on a design load obtained from a probabilistic approach. A different approach becomes more of interest namely that of Fluid-Structure Interaction (FSI). Until now, no FSI approach was applied on the Mark III corrugated panels.

Besides, the fluid behaviour on local scale (between two or three corrugations) has not been investigated.

knowledge gaps

Very limited research cases were applied in the field of LNG sloshing using FSI. Computational fluid cases are investigated using rigid walls. Computational structure responses cases are usually studied using very conservative design loads. Experiments that took place could

give much better insights in loads and responses. But, experiments are limited to physical measurements that can simply not show all behaviours. This leaves a certain amount of knowledge gaps;

- A clear insight in how pressures, at local level, develop when a wave interacts with the structure. Two dimensional and three dimensional.
- No data was obtained in Sloshel experiments measuring stresses along the corrugation. Two dimensional and three dimensional.
- Coupled interaction between fluid and mechanical models. This is the principle of Fluid-Strucutre Interaction.
- It is not verified, if incompressible Navier Stokes equations are able to describe the problem.

This set of knowledge gaps leaves enough research topics to tackle for which research questions are formulated in the next section.

1.3. Objectives and scope

Considering the knowledge gaps that appears to be, it will be the interest of this thesis to study the fluid behavior and structural response using a FSI approach.

The central question that will be red-wire in this research sounds:

What is the effect of FSI on a prediction of the plastic deformation of a Mark III membrane, subjected to a local wave impact?

The goals that will be achieved are:

- Verify a method that can be used for numerical FSI simulation, using a benchmark study.
- A model that is validated using the experiments of SLOSHEL.
- Analysis of the response of the structure due to different load cases.
- Determine whether the FSI two-way coupling between the fluid and structure is a significant benefit compared to a one-way coupling or no coupling, using numerical results.
- Compare design loads that are conventionally used for FEM to loads obtained from FSI.

The aimed product of this work is a validated numerical FSI model that simulates the loads and responses on Mark III corrugations.

Why is chosen for FSI simulation?

- It is possible to investigate what cannot be measured.
- Reduce the amount of physical experiments.
- Proactive designing instead of reactionary designing, by simulating experiments that not have been taken place in the past.

- Flexible structures demand for coupled time and spatial analysis in order to obtain reliable values.
- Numerical FSI opens opportunities for very complex loads and structures.

Scope

The constraints that describe this research are bounded by a research that focuses on the local impact of a wave on a Mark III corrugated membrane.

The software that is used for this simulation is a commercial package LS Dyna. This package involves a FEM fluid solver and a FEM mechanical solver, that are able to interact. It is chosen to use an incompressible CFD solver, which assumes the fluid to be incompressible and the gas medium around the fluid to be a vacuum. In chapter 3, the effects of this simplifications will be discussed.

The research topic was suggested by ClassNK (Japan), one of the classification society partners of SLING. The topic was approved by the program leaders, TU Delft and Marin. The SLING framework describes:

SLING focuses on the reduction of costs for ships through an optimal design of LNG cargo and fuel tanks within acceptable risk levels

The research directly contributes to this research goal, where we use FSI to determine whether or not fluid loading will damage the CCS within acceptable deformation (described as a risk).

As we know the fluid behaviour inside the tanks is highly random. Therefore experimental load cases as well as academic load cases will be used to study the structural behaviour. Two dimensional and, three dimensional models will be used in order to study fluid loading and structural response. In this study the focus will be on local impact. Meaning, that the model is limited to a few corrugations.

Models that are applied here, are validated with an experimental case that took place at atmospheric circumstances. Water was used as fluid (which has a density of approximately two times that of LNG). The materials that are used in the model to build the structure are the same for those that are applied in ships, corrugated membrane, plywood and foam; just as in the SLOSHEL Experiments.

1.4. Overview report

Theoretical aspects, that will be used for the method and analysis, are treated in chapter 2. In chapter 3 benchmark studies are described that are performed to determine the input parameters for the model. The model and the method that is applied for the analysis of the problem is treated in chapter 4. The analysis is described in chapter 5, after this chapter conclusions are drawn from this analysis. This can be found in chapter 6. The thesis closes with a list of recommendations made after this study chapter 7.

2

Theory

In this chapter the theory is described behind methods used in this thesis. A brief background on the mathematics and physics that is used in the solver is given. The chapter is divided in three sections: Fluid, Structure and Fluid-Structure Interaction. The software that was used for simulations in this research is LS Dyna. A description is given of the most important physics that is used for the simulations.

2.1. Fluid Models

The fluid behaviour that is simulated in this thesis, is based on the Navier-Stokes equations. Some simplifications are made, such as incompressible liquid. Also additional models were used in order to obtain stable solutions, this involves free-surface handling and turbulence models. In this section, the most important topics of the mentioned subjects are treated.

2.1.1. Navier-Stokes equations of incompressible flows

Most of the numerical solvers for fluid simulation, that are programmed today, use Navier-Stokes equations. The Navier-Stokes equations consists of a set of two partial differential equations[19]. The first equation describes the conservation of mass. The second equation describes the conservation of momentum Equation 2.1. The strong form of the Navier-Stokes equations of incompressible flows may be written as [7]

$$\frac{\partial(\rho\mathbf{u})}{\partial t} + \nabla \cdot (\rho\mathbf{u} \otimes \mathbf{u} - \sigma) - \rho\mathbf{f} = \mathbf{0} \tag{2.1}$$

$$\nabla \cdot \mathbf{u} = 0 \tag{2.2}$$

where ρ, $\mathbf{u}$, and $\mathbf{f}$ are the density, velocity, and the external force (per unit mass), respectively and σ represents the stress tensor. Which includes the pressure p, dynamic viscosity μ, and the strain-rate tensor ε.

It was stated valid by Batchelor in 1967 [6] to assume that a fluid is incompressible when the fluid velocity is much smaller than the speed of sound in the fluid. If the fluid velocity

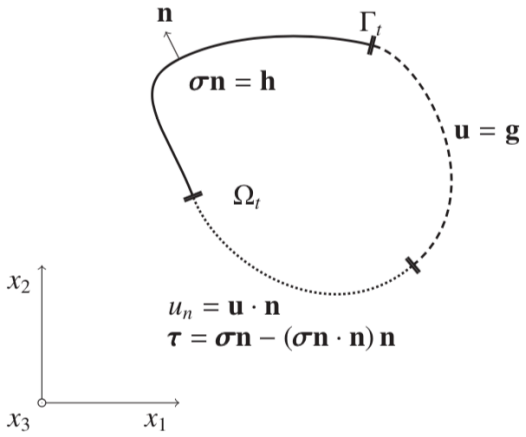

Figure 2.1: Description of fluid domain. [7]

is less than 0.3 the speed of sound, it is generally accepted that a fluid may be assumed to be in compressible [13]. This first simplification reduces the complexity of the Navier-Stokes equations.

Boundary- and initial conditions

Equation 2.1 is not complete, if no boundary and initial conditions are applied. At non-permeable walls, with free slip condition, boundary conditions describe a zero velocity normal to the surface. Besides, with non-slip condition, the tangential component equals zero additionally. One can describe this boundary condition as:

$$\mathbf{u} = \bar{v} \quad \text{on} \quad \Gamma_b \tag{2.3}$$

in which $\bar{v}$ indicates the function that is imposed on the wall (free- or non-slip). Γ_b describes the shape of the boundary.

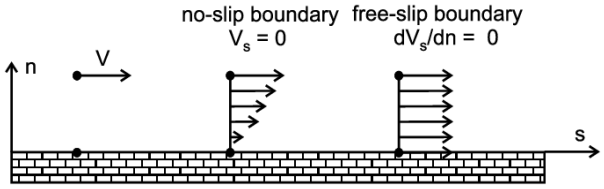

Figure 2.2: Non-slip and free-slip boundary conditions

The initial conditions for the Navier-Stokes problem are described by Equation 2.4. To solve the Navier-Stokes equations numerically, the solver requires at least an initial velocity, v_i^0, and an initial pressure p_i^0 at the boundaries. This should be defined for any location of the active fluid x_i. In which $i = 1, 2, 3$ referring to the directions x, y and z.

$$\begin{aligned} \mathbf{v}(\mathbf{x}, 0) &= \mathbf{v}^0(\mathbf{x}) \\ p(x_i, 0) &= p^0(\mathbf{x}) \end{aligned} \tag{2.4}$$

Free surface

At the free surface, it is assumed for the liquid to be separated from a gas. For the free surface two conditions should be satisfied. The first describes the stress tangential to the surface, which must be zero. The second condition states the stress normal to the surface that must exactly balance any externally applied normal stress.

$$\mathbf{t} = \sigma\mathbf{n} = \bar{t} \quad \text{on} \quad \Gamma_f \tag{2.5}$$

where $\mathbf{n}$ is the direction vector on the boundary. And, σ states the stress tensor and $\bar{t}$ stands for the stress traction at the free surface boundary Γ_f just in the fluid, where t_i stands for the stress just in the gas. It is considered that Γ_b from Equation 2.3 and Γ_f are disjoint non-overlapping subsets of the boundary Γ.

The solver of LS Dyna uses a level set method based on [30]. This method that is used to estimate the free surface of the fluid. This is a estimating method, therefore it contains an error term. The model is not mass conservative and very small fluctuations in fluid area can be observed.

The Elementary Loading Process

Based on experimental research, the wave interacting on a structure could be distinguished in three phases: the Elementary Loading Process (ELP) [8]

- Direct impact (ELP1)
- The building jet (ELP2)
- The compression of escaping or entrapped gas (ELP3)

2.2. Structure

In this section a brief background is given on the equations that are solved in the mechanical solver. Aspects such as material types and element types will be treated.

2.2.1. Basic mechanics

In beams and plates strains and stresses are distinguished. Strains are a results of displacements and stresses are a result of strains. Consider a simple solid element that is subjected to a force in all 3 directions. Than the normal strain is expressed by:

$$\epsilon_x = \frac{\partial u_x}{\partial x} = \frac{\Delta L}{L_0} \qquad \epsilon_y = \frac{\partial u_y}{\partial y} \qquad \epsilon_z = \frac{\partial u_z}{\partial z} \tag{2.6}$$

From strains the step can be made toward stresses using Hooke's law. This states that:

$$\sigma = E\epsilon \tag{2.7}$$

In which E represents Young's modulus. Now, to make the step towards stress in beam bending a small modification should be made.

$$\sigma_x = \frac{Ey}{\rho} \tag{2.8}$$

2.2.2. Element types

In FEM analysis different types of elements are distinguished; Solid-, Shell-, Beam- and Discrete- elements. Besides the type of elements, the number of integration points inside the element is variable and the number of nodes per element is variable.

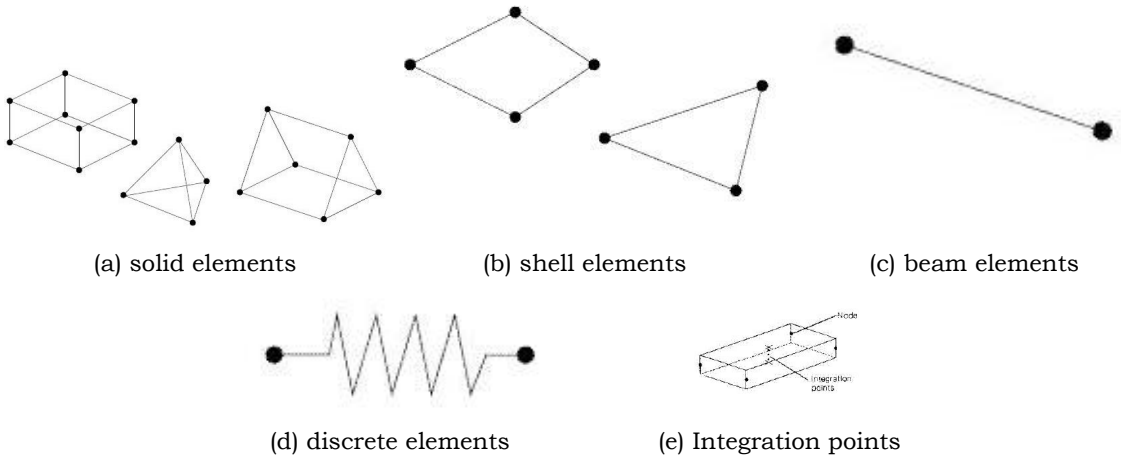

(a) solid elements (b) shell elements (c) beam elements

(d) discrete elements (e) Integration points

Figure 2.3: element types that are implemented into LS Dyna [37]

Increasing the number of nodes and integration points will require more CPU power. On the other hand, decreasing the number of nodes and integration points will decrease the accuracy of the calculation. A reason to choose for elements that contain many nodes and integration points, will increase the accuracy of that specific element.

In this research a benchmark study is performed on different types of elements. In this study it was found that shell elements for 3 dimensional- and beam elements for 2 dimensional analysis show optimal results in terms of accuracy versus computations time.

2.2.3. Material types

In this subsection an elastic-plastic model is used to mimic the behaviour of stainless steel. First the engineering stress-strain curve is compared to the true stress-strain curve Figure 2.4. In a tensile test specimens are subjected to forces that induce strain. Elongating in longitudinal direction induces shrinking in cross sectional area as is described with Poisson's ratio. After reaching the ultimate stress, the behaviour of necking occurs. Necking is the fast shrinking in cross sectional area and fast elongation in normal direction of the material, while the strain rate is constant. In a engineering stress-strain curve, only the initial surface of the specimen is considered. While, in true engineering stress-strain curves, changing area is considered.

The material that is used by LS Dyna is included strain hardening. It does not include the necking phase of the material, only the Poisson ratio is considered. Two types of hardening

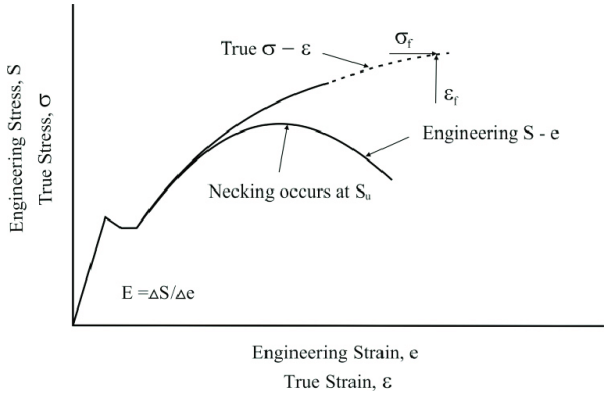

Figure 2.4: Engineering stress and strain curves [24]

are considered. Isotropic hardening and kinematic hardening. Isotropic hardening is a uniform yield surface expansion. Kinematic hardening is a shift of yield surface without change of size/shape. More detailed information about kinematic and isotropic hardening can be found in [33]

2.3. Numerical Implementation

The Fluid solver used by LS Dyna uses an FEM solving technique. This choice was made by the developer, because this will make it convenient to transfer loads from the CFD solver toward the mechanical FEM solver in a Fluid-Structure Interaction problem.

2.3.1. Time integration

The velocities in the model are approximated using an integration scheme with backward differences of second order.

$$\frac{d\mathbf{u}^{n}}{dt} = \frac{3\mathbf{u}^{n+1} - 4\mathbf{u}^{n} + \mathbf{u}^{n-1}}{2\Delta t} \tag{2.9}$$

In this equation $\mathbf{u}$ refers to the velocity. Δt is the time step for the simulation. In order to approximate the velocities one step further, u_i^{n+1}; a 3 steps method is used. Details of this method are described in [13].

2.3.2. Mesh Quality

The software LS Dyna is provided with an automatic mesh algorithm [13]. A user should check the mesh quality that is suggested by the algorithm. Two methods are most common to do so. The first technique is based on the aspect ratio of the elements that are created. The fluid solver of LS Dyna only uses triangular shaped elements. To examine the quality of the elements, the following criterion is used.

$$Q = \frac{L \cdot S}{V} \tag{2.10}$$

Where L is the longest edge, S is the surface area of the mesh element and V is the volume of the mesh element. High Q value means that the element mesh might be distorted and could lead to divergence issues. Q values less than 10 accepted. This value was determined by LS Dyna.

The second method refers to the Courant-Friedrichs-Lewy condition and is found by the same named scientists in their paper in 1928 [14]. Their condition is stated to be required in order to obtain convergence. The principle of the condition can be described by an example of a wave that is moving trough a spatial grid and one want to calculate the amplitude at discrete time steps of equal duration. Then the duration of one timestep must be less than the time for the wave to travel to adjacent grid points. For the one-dimensional case:

$$C = \frac{u\Delta t}{\Delta x} \leq C_{max} \tag{2.11}$$

The dimensionless number C is called the Courant number, u is the magnitude of the velocity, Δt is the time step and Δx is the length of the interval

If an explicit[1] solver is used then typically $C_{max} = 1$. Implicit solvers are usually less sensitive to numerical instability and so lager values of C_{max} may be tolerated.

2.3.3. Numerical Uncertainty

Numerical solutions are most likely to be an approximation of the analytic solution. First, a difference is made between uncertainty and error. Uncertainty is defined as:

'A potential deficiency in any phase or activity of the modeling process that is due to the lack of knowledge'

Error is defined as: *'A recognizable deficiency in any phase or activity of modeling and simulation that is **not** due to lack of knowledge.'*[5]

In CFD acknowledged errors are distinguished from unacknowledged errors [34]. In acknowledged errors, procedures are available for finding these errors, unacknowledged errors do not have procedures for finding them and will remain during the simulation.

[1]The fluid solver always uses an implicit solving method. More information about this topic can be found in the next section: Structure

Acknowledged errors

1. **Physical approximation error:** (Physical modelling error) these errors arise due to uncertainty of how to model the physics and also due to simplification of the models.
2. **Computer round-off error:** these errors deal with the limitations of computers, computers have a limit number of digits that is used to make calculations. This errors compared to other errors is generally not significant.
3. **Iterative convergence error:** Iterative convergence errors occur in implicit analysis. Equations that are solved in these equations are mostly non-linear and too difficult to solve exact, therefore iteration methods are used to find approximate solutions. By the user defined, the number of iterations or the accepted error is defined in order to limit the calculations
4. **Discretization error:** (spatial, temporal) the discrete spatial domain is know as the grid or mesh. Finer grids normally result in smaller spatial discretization error. The temporal discretetiation manifest through the time step. Smaller time steps in general results in smaller temporal error. Discretisation error is also known as the numerical error.

Unacknowledged Error

1. **Computer programming error:** these errors are the results of mistakes made by the programmer. Programming errors are the responsibility of the programmer.
2. **Usage error:** these are errors or mistakes made by the user of the software. One can obtain a converged model, but draws wrong conclusions. Usage errors can be decreased by training of the user.

Errors should be as low as possible and qualified. Iterative error and discretisation errors require methods to quantify the accuracy of the model. It was found by Eca en Hoekstra that iterative errors should be in the order of 2 to 3 times smaller than the discretisation error [16].

2.3.4. Structural models implementation

Before computers can solver our problems, mathematical methods are required to make it possible to compute solutions. One of these methods is the calculating explicit or implicit the next state of a system. In this section an introduction is given on the explicit and implicit solving method.

Consequence of using approximate methods is that errors will occur. Hour-glassing and Shear-locking are two examples of errors that will occur only in numerical analysis. These topics will be discussed.

2.3.5. Explicit and Implicit solving

Explicit methods calculate the next state of a system directly by making an approximation, using the data that is available at the current time step. Implicit methods find a solution by solving an equation involving both the current state of the system and the later one (in some methods also one step before the current state). Such equations and a more mathematical description can be found in

Explicit method

$$f(x^n) = \frac{x^{n+1} - x^n}{dt} \tag{2.12}$$

Implicit method

$$f(x^{n+1}) = \frac{x^{n+1} - x^n}{dt} \tag{2.13}$$

In LS Dyna, static analysis is done using an implicit solver. Dynamic analysis (where inertia does play a role), is performed using either explicit or implicit solving techniques. In explicit analysis, no iteration steps are required as the nodal accelerations are solved directly.

The time step in explicit analysis must be less than the Courant time step (described in previous section). Implicit transient analysis has no limit on the size of the time step. Therefore, implicit time steps are generally several orders of magnitude larger than explicit time steps.

Explicit analysis handles non-linearities with relative ease as compared to implicit analysis.

The principal reason for using implicit solution methods, which are more complex to program and require more computational effort in each solution step, is to allow for large time-step sizes. Numerical stability has to do with the behavior of the solution as the time-step dt is increased. If the solution remains well behaved for arbitrarily large values of the time step, the method is said to be unconditionally stable. This situation never occurs with explicit methods, which are always conditionally stable.

The choice of whether an implicit versus explicit method should be used ultimately depends on the goal of the computation. When time accuracy is important, explicit methods produce better accuracy with less computational effort than implicit methods.

In LS Dyna the fluid solver uses a implicit solving method and in the mechanical solver, most of the analysis is performed using an explicit solver.

Hourglass Control

Hourglass (HG) modes are nonphysical, zero-energy modes of deformation that produce zero strain and no stress. Hourglass modes occur only in under-integrated (single integration point) solid, shell, and thick shell elements. [15]

Consider an element with one integration point subjected to pure bending Figure 2.5

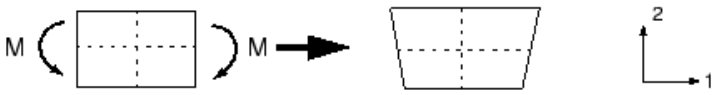

Figure 2.5: Deformation of a linear element with reduced integration subjected to bending moment M [36]

Neither of the dotted visualization lines has changed in length, and the angle between them is also unchanged, which means that all components of stress at the element's integration point, located in the middle of the element. This bending mode of deformation is thus a zero-energy mode because no strain energy is generated by this element distortion. The element is unable to resist this type of deformation since it has no stiffness in this mode. In coarse meshes this zero-energy mode can propagate through the mesh, producing meaningless results [3].

Shear locking

Shear locking is an error that occurs in finite element analysis due to the linear nature of quadrilateral elements. The linear elements do not accurately model the curvature present in the actual material under bending, and a shear stress is introduced. The additional shear stress in the element (which does not occur in the actual beam) causes the element to reach equilibrium with smaller displacements, i.e., it makes the element appear to be stiffer than it actually is and gives bending displacements smaller than they should be.

In areas where linear elements are loaded by in plane bending, shear locking is prevented by using preferably 3 elements over the height. More information can be found in [35]

2.4. Fluid-Structure Interaction

Two-way coupling refers to the way of information transfer, where pressures from the fluid solver are transferred to the mechanical solver. Than the mechanical solver calculates the displacements and transfers them back to the fluid solver. Than the fluid solver updates the pressures according to the displacements of the structure and sends them to the mechanical solver. This process iterates until there is a clear convergence. Criterion of this convergence is determined by the user and often it is based on stiffness convergence. The other coupling mechanism is one-way coupled. In this system the fluid solver treats the structure as non-deformable, where the structure solver is able to deform. This means that forces from the fluid solver will be transferred only in one direction towards the structural solver.

Fluid–structure interaction (FSI) is the interaction of some flexible structure with any fluid loading.

To explain the principle on how to solve FSI numerical, a wave impacting on a structure is used in figure 2.6. In this figure, five iterations of one time-step are shown. In this images, the fluid is solved using a CFD solver, the structure is solved using an FEM solver. Here five iterations of one time-step are considered. At first, the wave impacts the wall (a), the response of the wall is solved by the mechanical solver (b). Displacements of the wall are transferred to the fluid solver solver, so that the fluid can be updated in shape and pressure forces (c). Decreased forces are transferred to the mechanical solver, which updates the displacements (d). The next step is again an update of the fluid (e). The iteration solving process converges. Controlling the converging process is done by aiming for a minimal change between iteration steps.

Fluid-structure interaction can be solved analytically for simplified model cases. In many cases structural geometry or complex fluid loading, make that numerical simulation offers response with higher accuracy.

For the understanding the pressures of one-way coupled systems and two-way coupled systems, one could imagine two impacts: the first impact by considering the amount of pressure that is observed at a contact surface is higher when an impact force hits a brick rigid wall, compared to an impact on a flexible wall that will bend in the direction of the punch, in the second case the amount of pressure at the contact surface is much less compared. The brick wall should be assumed with the pressures one way coupled system, while the flexible wall should be considered as the pressures of the two-way coupled system.

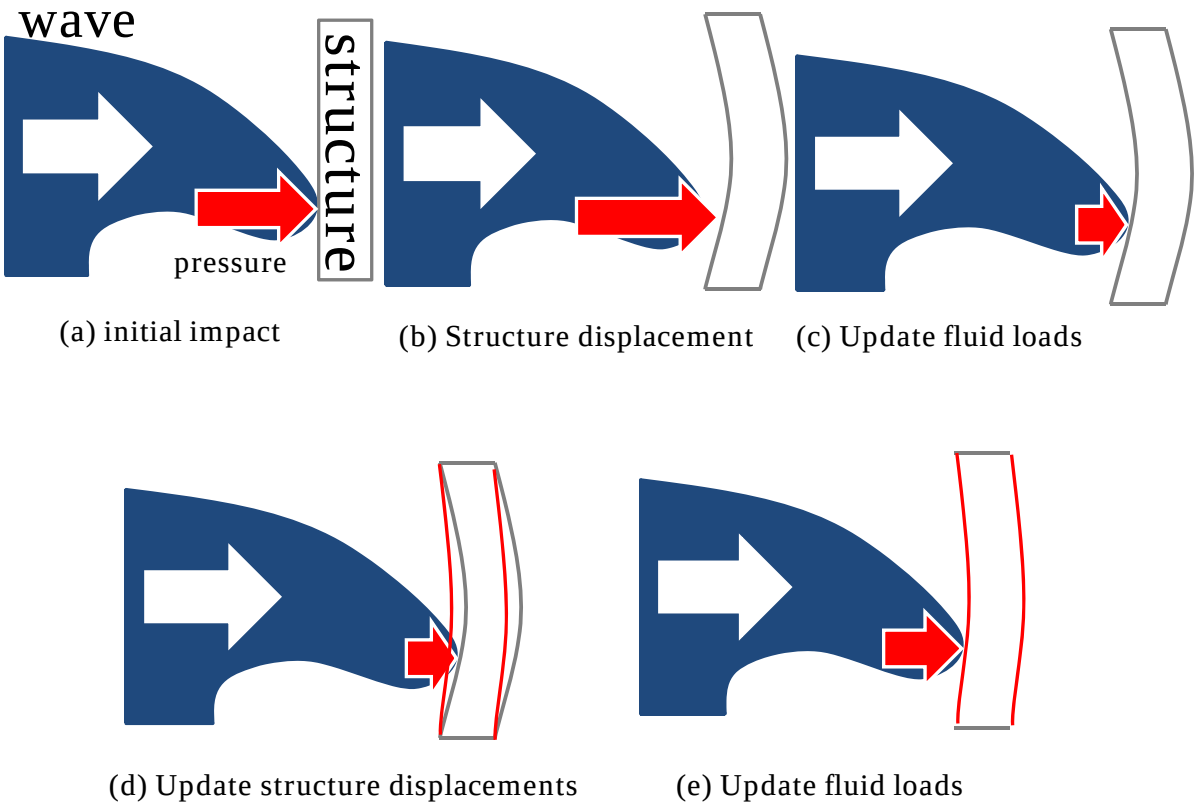

Figure 2.6: five iterations of one time-step

2.4.1. Monolithic and partitioned solvers

Monolithic solver use the approach of solving the equations governing the flow and the displacement of the structure simultaneously, with a single solver. When the Partitioned method is applied, the equations governing the flow and the displacement of the structure are solved separately, with two distinct solvers.

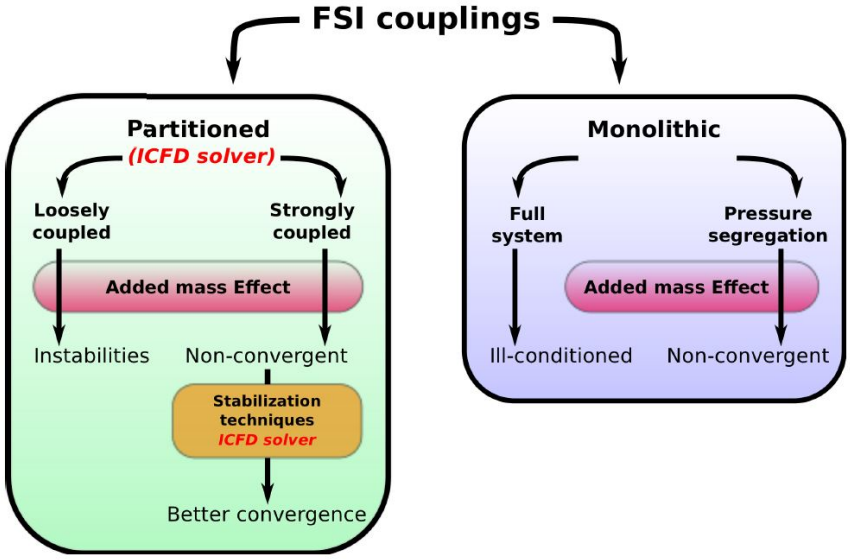

Figure 2.7: Partitioned solver scheme (left) and monolithic solver scheme (right) used by LS Dyna [20]

When added mass is considered in a model, monolithic solvers show non-converging solutions. Since, in most FSI problems, added mass is significant, the choice of a partitioned solving techniques is made by LS Dyna to implement this into the method.

2.4.2. Arbitrairy Euler Lagrangian

Arbitrairy Euler Lagrangian (ALE) is a technique often applied in numerical FSI. This method description refers to the way grids are treated in the numerical solvers. Eulerian grids or meshes refer to a domain that completely is solved for the full domain. The eulerian grid points are fixed in space. An example of an Eulerian grid is a CFD simulation in which the complete domain is computed each time step. The Lagrangian description on the other hand, is a grid that moves with the deformation of the shape of the object. Lagranginan grid points are able to move in space. An example of a Lagranginan grid is a structure that is exposed to an external force. The grid will move with the deformation of the structure.

A third possible case is the combination of these two. In FSI the fluid domain is described by Eulerian grid points and the structure is described by Lagrangian grid points. This combination is called arbitrary Euler-Lagrangian (ALE) and the Eulerian point are in this case able to move elastically. Like a spider web that is elastic and able to move freely by wind blowing through.

2.4.3. Coupling

The coupling method describes the way how the meshes of the fluid-solver and the structure-solver communicate their changes. The most conventional way is the fluid solver that transfers forces and pressures to the structure solver. Two schemes are distinguished. The loosely of weak coupled system and the strong coupled system Figure 2.8a. The loosely coupled schemes transfers only once information from the fluid solver to the mechanical solver and back each time step and require no iteration. Time step size consequently does not require to have the same time step for the separate solvers. This technique requires less computation power than the strong coupled scheme.

The strong coupled scheme iterates each time step until the desired level of convergence is obtained. The strong coupled system delivers the best results, but takes the most computational time.

The above mentioned coupling schemes are both two-way coupled systems. One could simplify the calculations by introducing a one-way coupled system. This means that either just the fluid solver transfers forces towards the mechanical solver, but no response of the mechanical solver is transferred backwards to the fluid solver. Consequently, the mechanical solver can transfer in one direction displacements, without feedback of the fluid solver.

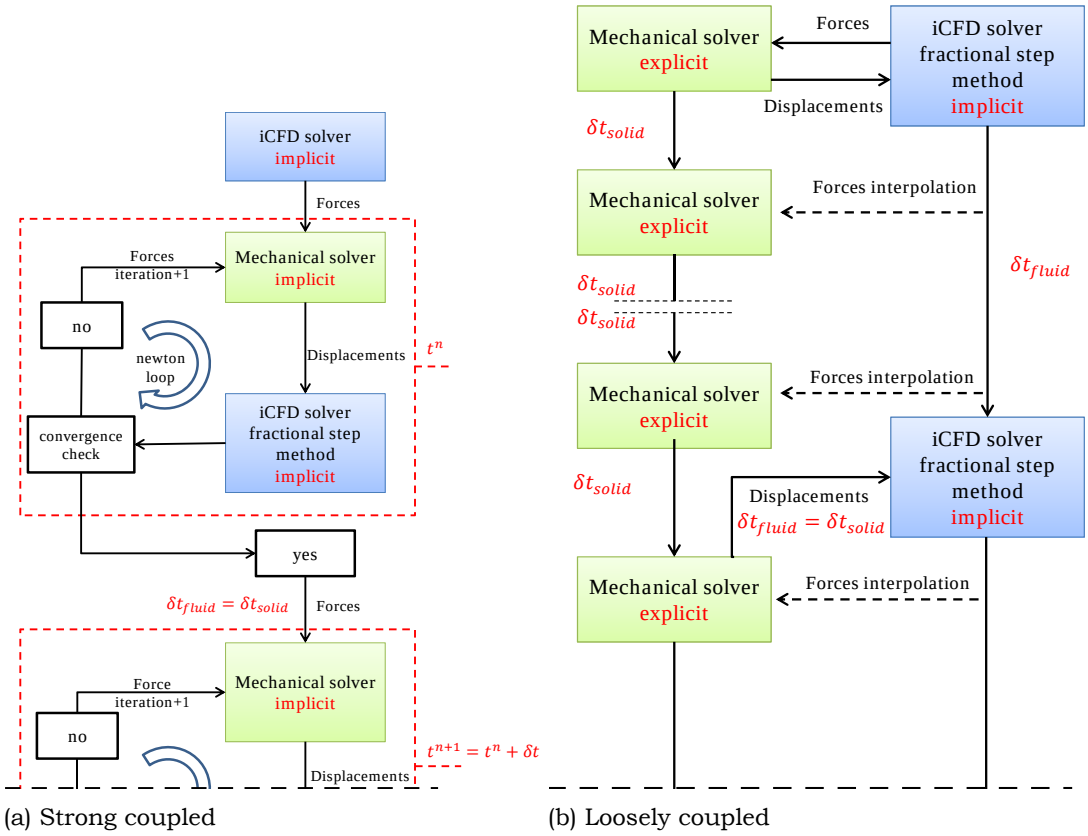

(a) Strong coupled (b) Loosely coupled

Figure 2.8: Strong and weak (loose) coupled schemes used by LS Dyna [20]

3

Benchmark

Four types of benchmark studies have been carried out. The first contains a benchmark focused on selecting an appropriate method for simulating a local impact wave, using a dambreak simulation. Then, the best modelling method is being benchmarked on different grid properties. The third benchmark was performed to test the reliability of the structural solver in LS Dyna. The chapter closes with a benchmark on Fluid-Structure Interaction, applying a flexible flap inside a flow channel, results of this benchmark are compared to results of other numerical simulations.

3.1. Modeling technique

A large variety of methods for modelling fluid is available. To decide which of this modelling techniques fits best for the local wave impact, several techniques are considered. The choice of software was made to be on LS Dyna, which supports several modelling techniques concerning FSI problems. LS Dyna consists of partitioned solvers in which fluid and structural behaviour can be simulated. The techniques that are considered are:

1. Arbitrairy Eulerian Lagrangian (ALE)
2. incompressible Computational Fluid Dynamics (iCFD)
3. Smoothed Particle Hydrodynamics (SPH)

ALE is discussed in the previous chapter and relates to the manner that different grids interact to each other. The fluid grid in this case does take into account the property of air, in contrast to iCFD.

iCFD relates to a technique implemented in LS Dyna based on FEM. Compressiblility is not taken into account. This reduces the amount of calculations that should be performed to simulate the model, leading to significant lower computation times. The second important property is that gas flows in a free-surface analysis, are considered as a vacuum [13].

Smoothed Particle Hydrodynamics (SPH) is a technique that does not require a grid [27]. This technique was initially invented in 1977 to model astrophysics. The method is particle based and uses a kernel function, i.e. all particles near each other interact with each other. The method can be applied for fluids and for (flexible) solids.

Three dam break models are built to analyse the behaviour of the different techniques. Dimensions of the model are 584 x 584 mm and the water column has a width of 146 mm and a height of 292 mm. For all the models, pressures are measured at five locations. In none of the models, surface tension is included and the gas (air) in the models are modelled as a vacuum. The only force that is applied is gravitational force. The ALE model uses a Eularian description of the fluid and gas, where the boundaries of the wall use a Lagrangian mesh description, see Figure 3.1 middle. The SPH model uses a single layer of particles in which 61 particles are used in the x-direction and 121 in the z-direction.

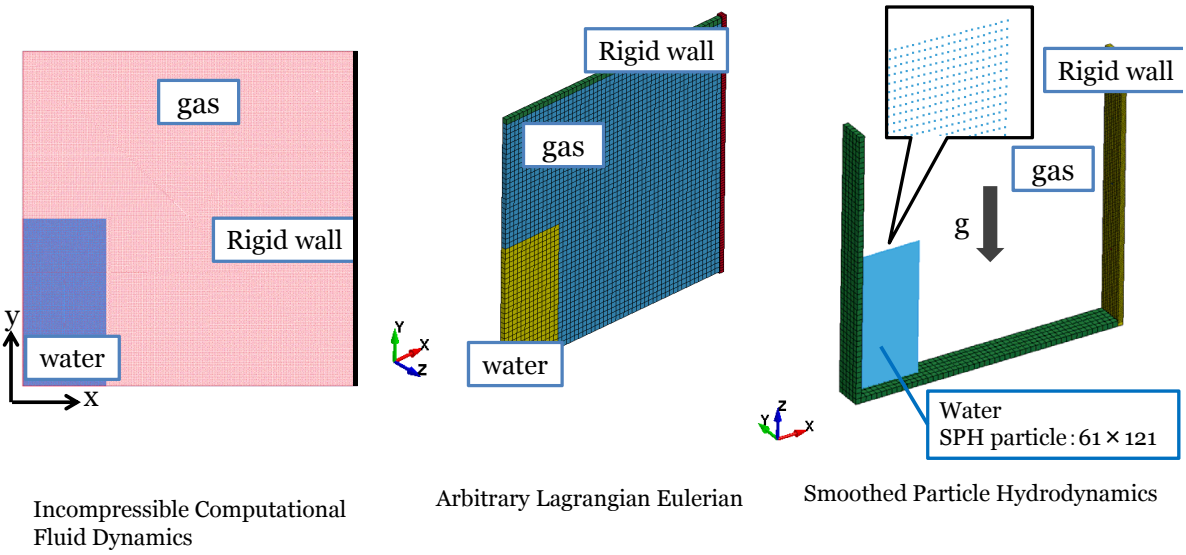

Figure 3.1: Three methods for a dam break simulation. Density liquid: $998 kg/m^3$, density gas: $1.205 kg/m^3$, viscosity: $1.002 Pa \cdot ms$, gravitation: $9.81 m/s^2$

Dam break experiment

The dam break experiment has been recorded by [26]. In this experiment a column of water is hold by a walls of a small basin and a thin layer of wax. The thin layer of wax was exposed to electricity, which melts the wax and therefore the water column was only exposed to gravitational force. The dambreak simulation was recorded with a camera at 300 frames per second.

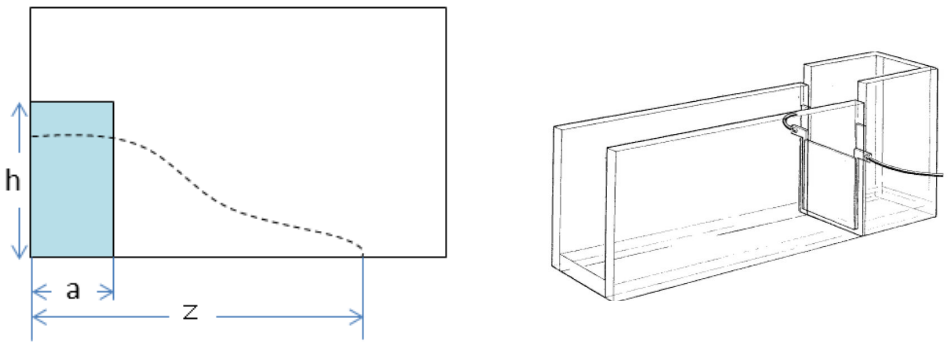

Figure 3.2: Left: dimensions of the dambreak experiment. Right: apparatus of the dambreak experiment used by [26]

During the collapse of a fluid column, the following relation holds.

$$z/a = F[n^2, t(g/a)^{\frac{1}{2}}] \tag{3.1}$$

In which, z is distance of surge from from axis, a is the dimension of characteristic of column base, $n^2 a$ is the original height of the column (note that $n^2 = 1$ give a square column), t is time and g is the acceleration due to gravity.

The post processing of these experiments contains some dimensionless numbers, from which the experiments can be compared with simulations.

$$Z = z/a \tag{3.2}$$

$$H = \eta/an^2 \tag{3.3}$$

$$\tau = t(g/a)^{1/2} \tag{3.4}$$

$$T = nt(g/a)^{1/2} \tag{3.5}$$

$$n^2 = h/a \tag{3.6}$$

For comparing experiments to simulations two fluid motions are considered. 1) the horizontal motion that is moving away from the initial column, 2) the vertical motion in which the highest point of the water column is considered and will move downward. The results of two experimental for horizontal Figure 3.3, and one case for vertical motion cases are shown in Figure 3.4.

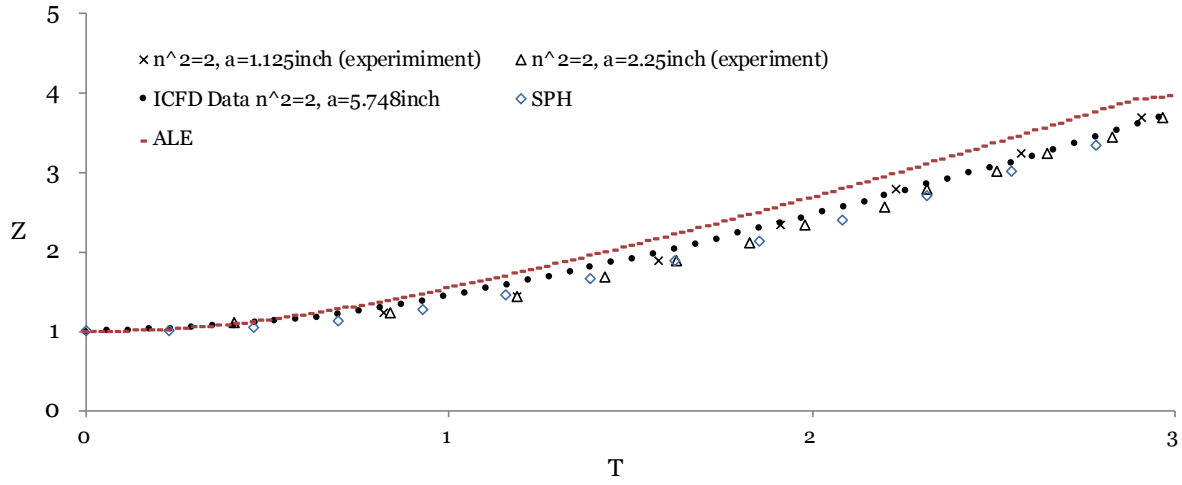

Figure 3.3: Results fluid behaviour dimensionless horizontal motion vs. dimensionless time.

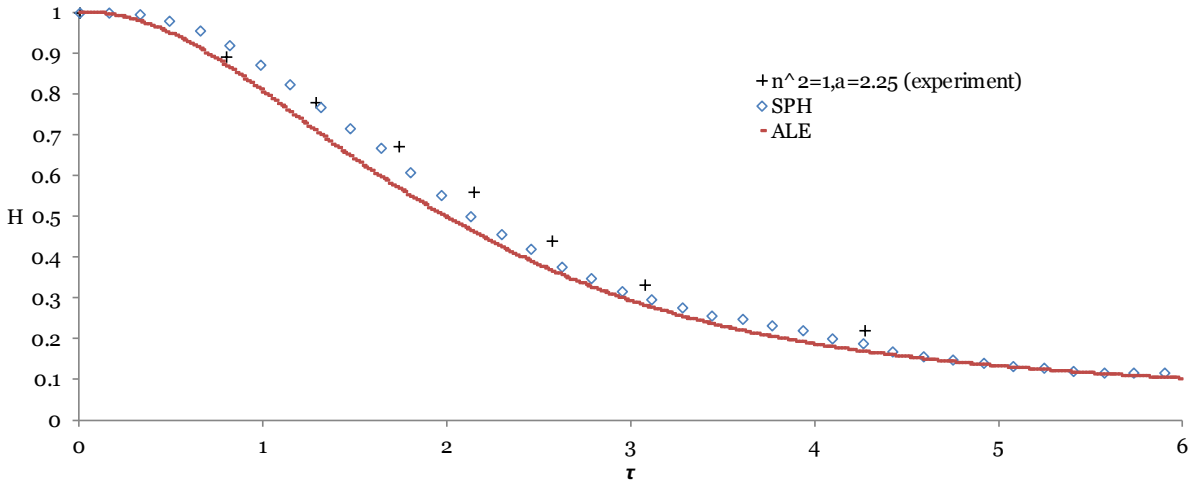

Figure 3.4: Results fluid behaviour dimensionless height vs. dimensionless time

The results of experiments are carried out for a column with a aspect ratio of $2^{1/2}$, this is similar for the simulations that have been performed numerical. The bandwidth of the experiments is narrow and therefore useful for comparing it to numerical results. The initial column of the numerical simulations is larger than the experiments, but due to the use of dimensionless numbers and the governing equations, it is possible to compare the results. Good fits on the horizontal motion have been obtained by iCFD and SPH, since these points show overlapping behaviour with the experiments. The ALE simulation shows a curve that is slightly higher than the experiments, which results in a slightly faster motion of the fluid.

For the vertical motion Figure 3.4, a similar behaviour is observed. The data for SPH is overlapping quite well, where the curve of ALE is shifted downward. This relates to a slightly faster moving fluid.

The second parameter that are tested are the pressures measured on the vertical wall. In Figure 3.5 the pressures at the bottom of the vertical wall on the right hand side of the model are shown.

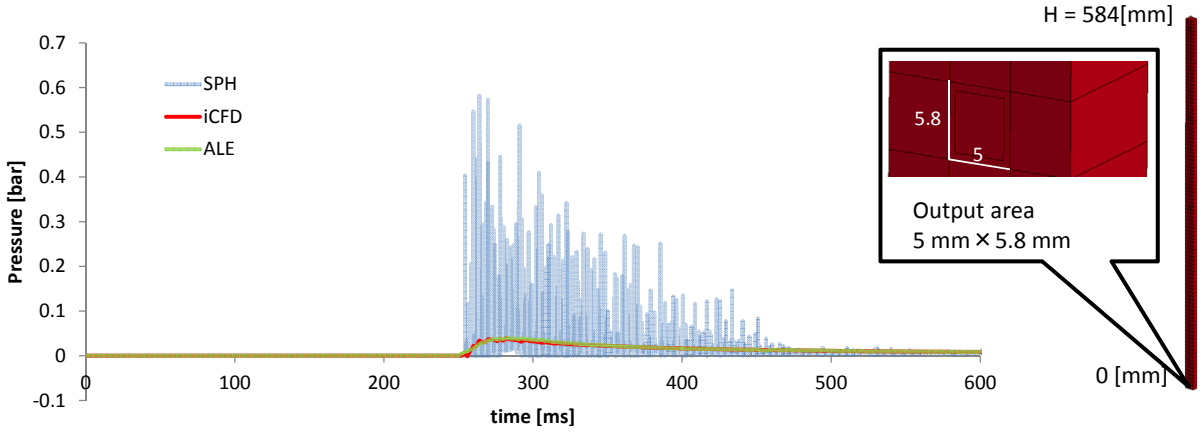

Figure 3.5: Dambreak simulation pressure results measurement point at lower right side

From this graph one can see that SPH has a very coarse behaviour. This is due to the impact of all the small particles interacting with the wall. Both iCFD and ALE results show overlapping and more smooth behaviour. This is desired for FSI analysis, because convergence is obtained faster with more steady pressures.

At last computation times are considered. This relative simple dam break model should deliver promising computational times, since it is only a part of the later developed FSI models.

Table 3.1: Computation times for the three different models

CPU times (8 cores)	
ALE	4 hours
iCFD	45 minutes
SPH	9 hours

Table 3.1 shows that iCFD uses the lowest computation time (45 minutes) compared to the 4 and 9 hours for ALE and SPH respectively.

Based on the benchmark that has been performed on the relative simple dambreak case, it was decided that iCFD will become the technique that is applied to model the FSI: iCFD shows a good fit compared to experiments on fluid flow behaviour, it shows reliable pressures that do not have a coarse behaviour and the computation time is low, enabling for this research to create fast and reliable results.

3.2. iCFD Dambreak Benchmark

A more detailed benchmark will be performed on the iCFD model that has been created. Dimensions were defined as can be seen in figure Figure 3.6 in wich $a = 146mm$

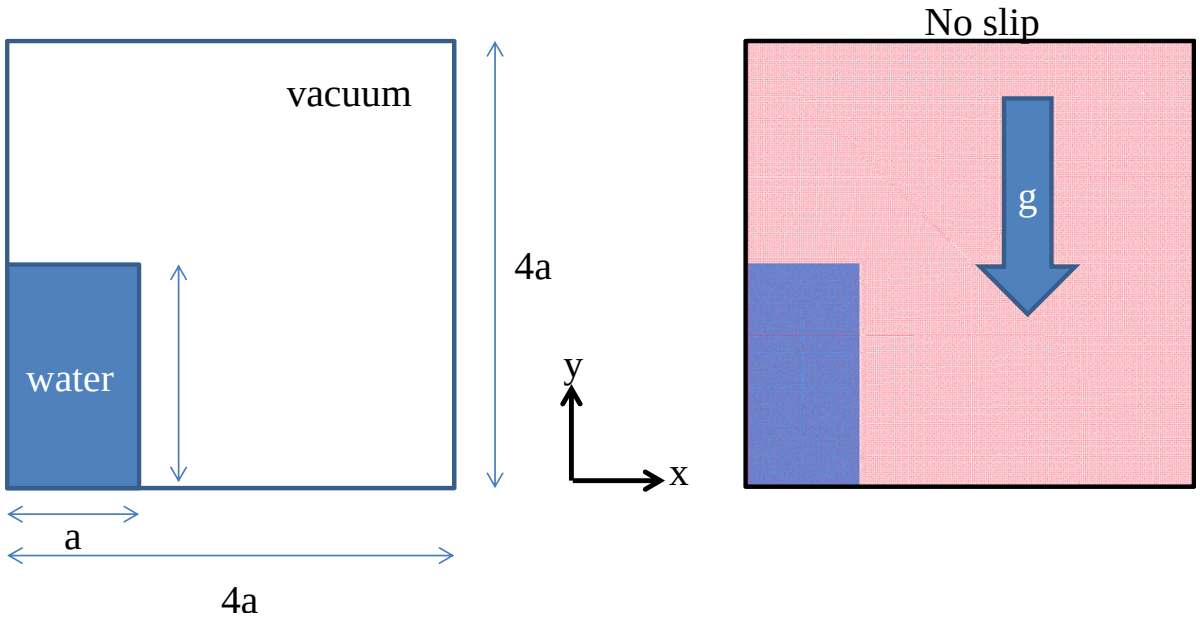

Figure 3.6: Dimensions, load and boundary conditions for the dambreak simulation

In Figure 3.6 it is shown that gravitation is active. Total width and height of the domain is: 584 mm. At the interface a level set method is active and all walls have a no-slip condition, since it is expected that the fluid velocity is low, therefore the Reynolds number is low and a development of a boundary layer is expected.

Grid study

In this case, the time step was kept constant, while the element size changed. Figure 3.7 shows the convergence behaviour of the simulations that have ran at different element sizes. The size E40 corresponds to 40 elements in x-direction and 40 elements in y-direction. The results of the different grid sizes were compared to the results of [26].

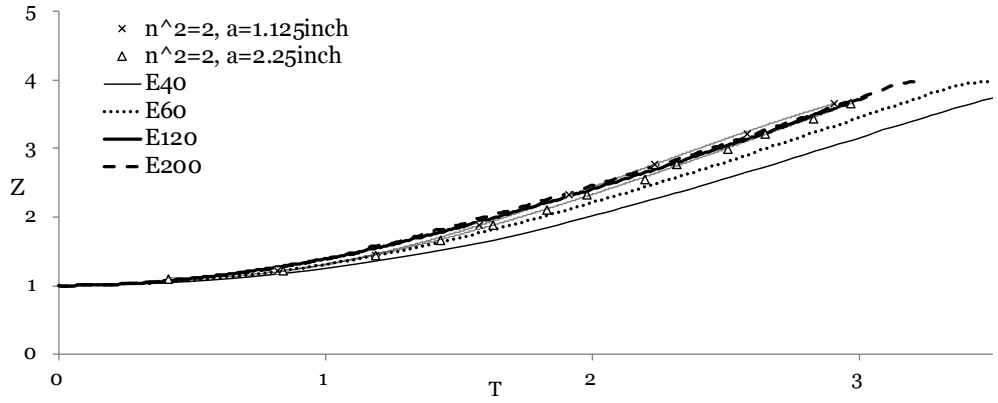

Figure 3.7: Results grid study. Convergence at 120 elements in x-direction and 120 elements in y-direction

For grid sizes E40 to E120 converging behaviour towards experimental values was observed. One step further at size E200 no significant improvement on convergence could be observed. So, 120 elements per side was good for this calculation. Note that a grid study for each model newly created model is required, and will be performed in further analysis.

Boundary Layer refinement

The boundaries of the walls were set to no-slip condition, which initiates a zero velocity at the wall. It was observed that gridsize is a very sensitive parameter for calculating a boundary layer near the structural boundaries in the fluid. Therefore the addition of extra grid refinement near the boundaries is considered and the results are shown in Figure 3.8

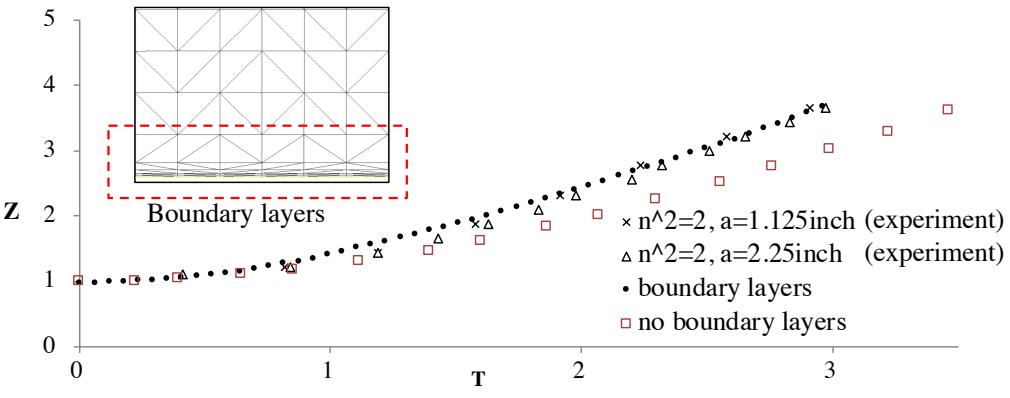

Figure 3.8: additional grid cells at boundaries

From these results, it is observed that no boundary layer mesh refinement shows a curve on the horizontal motion of the fluid that has a slightly less steep curve. This can be translated into a slower moving fluid. With the addition of extra grid elements near the boundaries of the fluid, the results overlap good compared to experiments. From this analysis it is taken that boundary layer refinement increases the accuracy of the fluid behaviour near the boundaries.

3.3. Structural Benchmark

The structural part of the solver is being tested using a fixed-free beam model that is subjected to a slow (static) load case and a fast (dynamic) load case using a distributed load.

Beam-, shell- and solid elements have been modelled in the structural solver. Solid elements are likely to give the best representation of analytic models. Although, shell and beam models give as it will be shown very accurate results and are much more economical in terms of CPU time.

Dimensions of the beam are shown in Figure 3.9. The beam has a length of 1m and has a thickness and width of 0.01m. At the lower end it is completely clamped and the load is applied on the nodes, which is equal to 0.5N. The material is artificial, it has somewhat of the material properties of that of plastic cups.

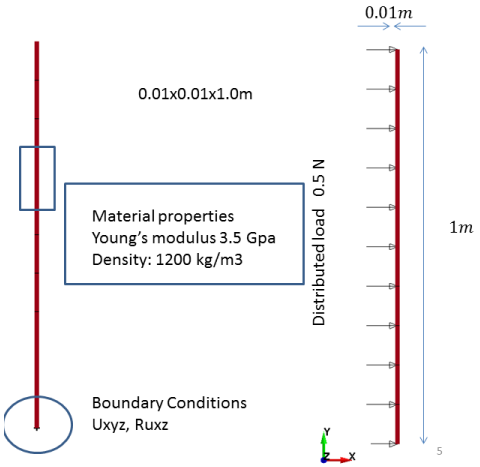

Figure 3.9: Input of the structural benchmark. Material properties, dimensions of the beam and load.

It was found by [11] that solid elements should have an aspect ratio near to 1, this is confirmed by [20]. Also, beam elements should be long and slender and also that shell elements should have an aspect ratio as close to 1.

The analytical solution is based on Euler-Bernoulli beam theory. For a fixed-free case in the first vibration mode, this becomes for the frequency 2.753 Hz.

$$f_n = 1.875\sqrt{\frac{EI}{\rho A l^4}} \tag{3.7}$$

Consequently for static analysis, the maximum deflection at the tip of the beam 21.5 mm:

$$\delta_{max} = \frac{ql^4}{8EI} \tag{3.8}$$

The distributed load was loaded with a rise 3 seconds for the static analysis and of 0.1 sec and decreases also from full load to 0 in 0.1 second for the dynamic analysis. The material model that is applied is an isotropic material.To make beam and solid models on the XY-plane, the nodes of models have to be constrained in z-direction and for rotation in x and y direction.

The results for a single case are shown in Figure 3.10. In which the frequency of the dynamic response are obtained using Fast Fourier Transformation. All calculations are performed using an implicit time integration method.

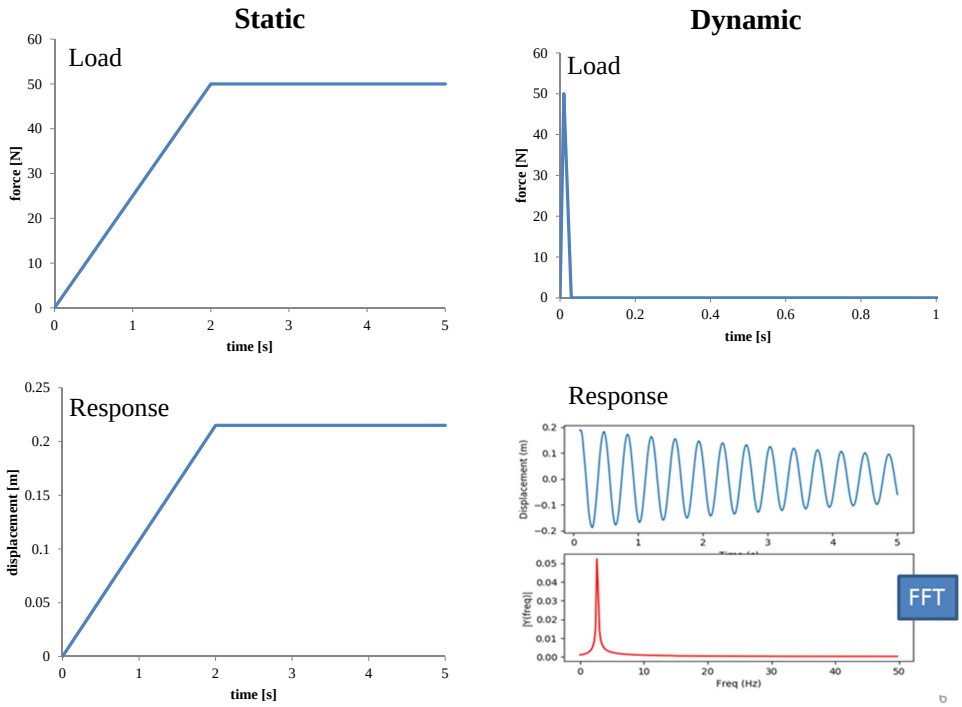

Figure 3.10: Static and dynamic Load and response of the structural benchmark case

From this single output file it can be seen that the static response clearly follows the static load case and the dynamic case hits a frequency that damps out in time. FFT analysis show clearly one peak that can be used for determining the first eigen-frequency.

Results of different beam-, shell- and solid elements are obtained and displayed in Figure 3.11.

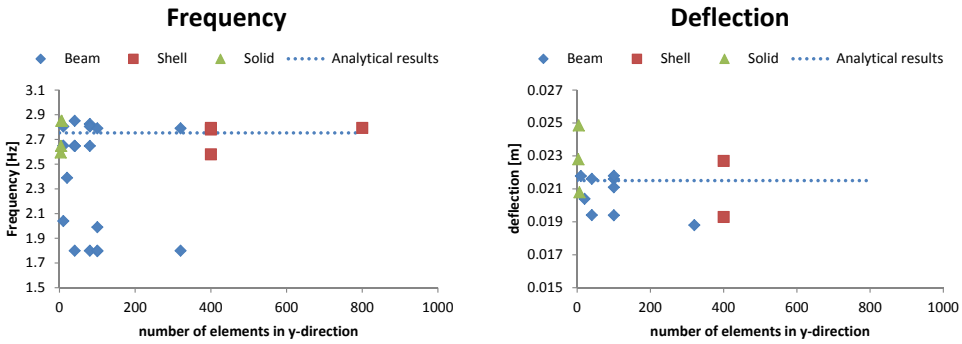

Figure 3.11: Left: dynamic responses for different element types. Right: static responses

Shell elements were tested. Different mesh sizes are applied and convergence was found. Also different mesh types were tested: triangular and rectangular. Triangular shapes were found to be faster and converge at larger element sizes.

Beam elements were used to build the model. Several different element types were tested, o-shaped, square shaped and hexagon-shaped cross-sections were considered. From this was found that only one element type suited well with analytic results. It was found that increasing the number of beam elements reduced the numerical error. Although, the length

to width ratio of the beam should have a long and slender characteristic. An optimal aspect ratio was found about 2.5.

And last, solid elements were tested in the model. These models show low errors compared to analytical results even with large elements. The number of integration points in solid elements is larger, consequently the number of calculations performed by the structural solver increases and much higher calculation times were measured.

It was found, that beam, shell and solid elements converge all to analytic results. All elements get near the analytic solution less than 4 percent. Although strong differences were observed for computation times.

3.4. Summary and conclusions

Two benchmark studies have been performed, one on the fluid behaviour and one structural behaviour. The following conclusions could be drawn from this study:

- The technique that will be used for further analysis is iCFD. A dam break benchmark study has performed comparing three techniques. ALE, iCFD and SPH. Best convergence on pressure and fluid motion was obtained using iCFD, besides the computation time of iCFD is the lowest.
- At a certain grid size, the fluid motion of the dambreak simulation does not converge any further. The size of the elements is 3mm, which gives an indication for the required gridsize that should be used in further analysis. Besides, a refinement of elements near the boundaries shows better results near the boundaries.
- For beam elements in the structural solver should be long and slender, an aspect ratio of 2.5 is found to give good results. For shell elements the aspect ratio should be as close as possible to one (squares).
- For thin structures in 2D analysis, beam elements show a good balance between accurate results and limited calculation times. For thicker structures solid elements will be used for calculations.

4

The Fluid-Structure Interaction Model

In this chapter, input parameters for the FSI model are discussed. The chapter is divided into two parts: 4.1 Model input, in which fluid- and structural solver are treated, 4.2 Results, in which the model is being validated using results that are obtained from experiments performed in SLOSHEL JIP.

4.1. Input Model

In this section the input variables for the models are discussed. The fluid model and the structural model are discussed separately.

4.1.1. Fluid model

In this case a flip-through wave is considered Figure 4.1, which impacts between two corrugations. The wave splashes on the wall, this induces a jet. The jets hit the corrugation first, followed by the water column. An analytical model and further explanation can be found in [32], in which the behaviour is similar to a crack filling flow.

Fluid properties

The fluid solver makes use of incompressible Navier-Stokes equations. The initial shape of the wave has been taken similar to the shape of the wave in experiments, using contour analysis. As can be seen in Figure 4.1 the water in experiments is highly consistent of air bubbles. Due to the bubbles, density of the fluid hardly changes while the speed of sound is affected: compressibility is $1/(\rho c^2)$. This makes the aerated fluid compressible. It is chosen to simulate the fluid as an incompressible fluid. This will affect the behaviour of the fluid: the effects are cushioning effects, but also pressure waves. Assuming that there is no effect of resonance, incompressibility will overestimate the forces. Besides, the gas in which the fluid flows, is considered as a vaccuum. The main reason for making this simplification, is that it decreases the amount of CPU time significantly, because then it is not required to solve a density-pressure equation (Equation of State). The density of the fluid is constant As will be shown in this section, the pressures that have been measured in experiments, overlap good with pressures that have been calculated in the simulation.

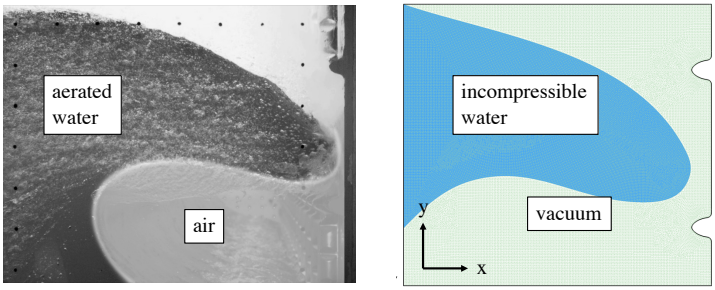

Figure 4.1: Left the experimental case. Right the model simulation

Density and viscosity values are used for 20 degrees Celsius. The surface tension is not taken into account. The reason for this is that the impact velocities are high. This leads to a high Weber number. The Weber number relates inertia forces to surface tension, in which high Weber number (Equation 4.1) corresponds to dominant inertia forces. Considering Table 4.2, Froude numbers are low at the initial impact due to the high characteristic length. For the characteristic length, the radius of curvature is taken at the front of the wave. Low Froude numbers, indicate the contribution of the gravitational effects versus the inertia effects. Therefore, gravitation is taken into account in the equation.

$$We = \frac{\rho L v^2}{\gamma} \tag{4.1}$$

$$Fr = \frac{v^2}{g L_{char}} \tag{4.2}$$

Table 4.1: fluid properties as defined in the model

density	ρ	998.2	kg/m^3
viscosity	μ	0.001002	$mPa \cdot s$
surface tension	γ	0	mN/m
gravitational forces	g	9.81	m/s^2

The Weber number is calculated at three stages. One is at the initial shape of the fluid, second is at the forming of the jets and third is after impact, when the jet is released from the corrugation after impact after enclosing. This last stage has shown to be less important since the pressure peaks at the moment of impact and not after the moment of impact. For finding the response of the structure, this is of minor importance.

Table 4.2: Fluid properties in three stages of the local wave impact

	Wave	**Jets**	**Spray (after enclosing)**
velocity [m/s]	7	20	30
L_{char} [m]	0.15 (radius of cruvature wavefront)	0.006 (thickness jet)	0.01 (thickness jet
Fr	33	6800	9200
Re	105000	120000	300000
We	100000	33000	123000

Gridsize and timestep

For the grid size a convergence study has been performed. The parameter that was used for determining the grid size is pressure Figure 4.2. The spikiness of the signal was considered and finally the pressures are compared to the experimental data that was obtained in SLOSHEL Joint Industry Project [8]. For the fluid grid triangular elements are used and an automatic meshing method is applied. For meshing algorithms it is more convenient to use triangular shaped elements, but is more difficult to organise the data. Besides with triangular shaped elements, orthogonality is achieved less often, which reduces the quality of the grid. It is necessary to judge the quality of the mesh. Initially the aspect ratio is being checked. Long shaped triangles are sensible for being passed by fluid velocities if the length of the cell is less than the local velocity divided by the timestep. The CFL number indicates if this behaviour takes place [see chapter 2]. If the CFL number in the cell is larger than 0.9, the the cells are too small and the time step should be decreased.

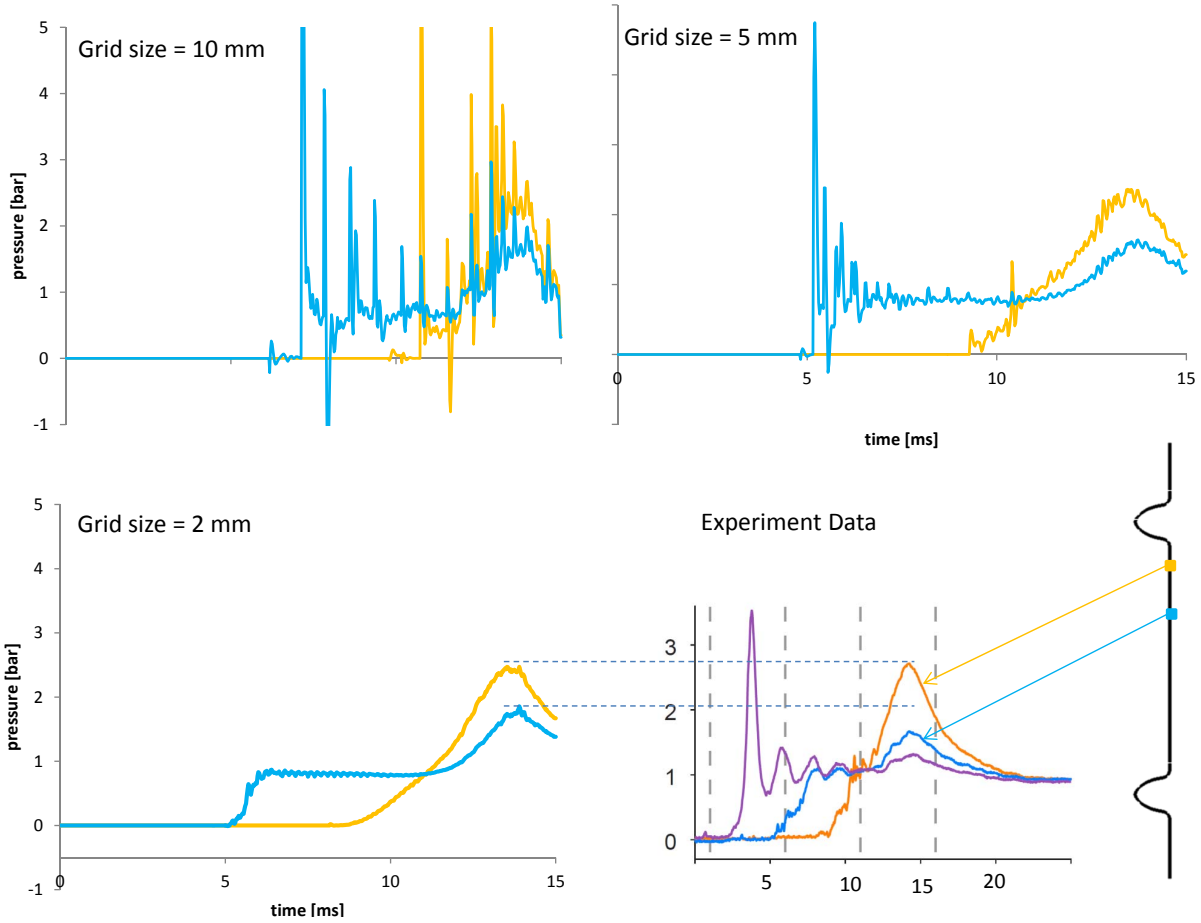

Figure 4.2: Pressure response of 2 locations for 3 different grid sizes 10, 5 and 2mm. As the gridsize reduces the spikiness reduces. The 2mm grid-case is compared to Experimental data [8]. Note that a third measure point in the experimental case was not taken into account in the simulations

In the grid study see Figure 4.2, three different grid sizes are used to simulate the wave impact. 10, 5 and 2mm. The sizes correspond to the initial distances between nodes on the boundaries. A automatic mesh algorithm fills the complete domain in which the maximum length of 10, 5 and 2mm are respected for the faces of the triangle With decreasing the grid size, the spiky behaviour of the pressure signal is significantly reduced. The simulation with the smallest grid size (2mm) is compared to the experimental results. The results are comparable. The peak of the pressures, in the graph measured between 10 and 15 ms, show similar or higher values for the simulations.

The timestep is dependent on the CFL number. For determining the timestep, a similar timestep is chosen as the measurement frequency of the experiments, so that both outputs could be compared to each other. The timestep that is used in analysis is $2 * 10^{-5}s$. This timestep is so small, that CFL numbers are very low. Later for coupling and stability reasons, the time step is held constant, as will be explained in the next section.

Table 4.3: Input variables used for the fluid model

gridsize	$2mm$
timestep	$2 * 10^{-5}s$

Boundary and initial conditions

For the initial conditions an estimation is made on the initial velocity at which the wave is approaching. This is set at 7 m/s. This value is obtained using contour analysis of the fluid experiments. Contour analysis is a fairly rough method to estimate the velocity and direction of the fluid. A better approach would be to use PIV, in which velocities, and directions of the fluid could be obtained with much higher level of detail.

The left hand side of the fluid domain has a fluid inlet in positive x-direction at a velocity of 7 m/s. The remaining boundaries, that are initially dry, have a free-slip condition. Additional the corrugated side on the right hand side, is set to be sensible for FSI i.e. this is the FSI interface. The other boundaries are non-penetradable (solid).

There is no time to develop a boundary layer, therefore free-slip condition (no wall shear stress) is applied on all boundaries. The reason for this can be found the reynolds number with boundary layer development and can be found in Appendix A

4.1.2. Structural model input

The structural part of the model is divided into three parts. 1) the corrugated membrane, 2) the plywood, 3) the foam layer.

Dimensions of the foam are similar to Figure 4.3, [Bos 2019, unpublished].

Material properties

For the plywood and for the foam an isotropic material model is used. For the corrugated membrane, also an isotropic material model is used including a plastic strain model. The idea of this model is described in Figure 4.4. Here we see that the tangent modulus, E_t, is active when the yield stress criteria, based on Von Mises stress, is exceeded. The hardening modulus β describes the amount of hardening that is induced by isometric hardening or kinematic hardening.

Grid properties and timestep

Since the shape of the grid is more complex than the grids in the benchmark cases, additional checks are performed. Such as the aspect ratio of the grid, which should not exceed 3, for triangular and rectangular cases in order to achieve a high quality grid.

The element sizes are obtained from the results of benchmark study in the previous section. The timestep is the same as used in the fluid solver in order to obtain faster a strong coupled

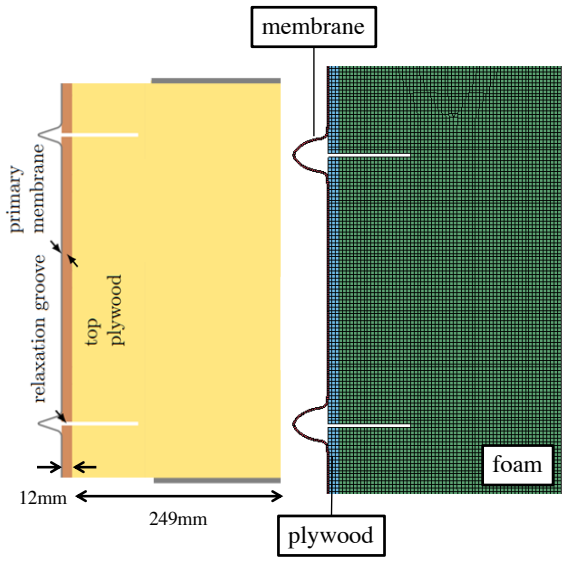

Membrane			
Youngs modulus	E_m	210	GPa
density	ρ_m	680	kg/m^3
Poisson ratio	ν_m	0.3	-
Yield stress	σ_y	240	MPa
Hardening parameter	β	0.45	-
Plywood			
Youngs modulus	E_p	7700	MPa
Density	ρ_p	680	kg/m^3
Poisson ratio	ν_p	0.3	-
Foam			
Youngs modulus	E_f	55	MPa
Density	ρ_f	125	kg/m^3
Poisson ratio	ν_f	0.2	-

Figure 4.3: Input structural model. Input parameters from [31] (density, Poisson ratio), [21](elastic modulus), dimensions from [9]

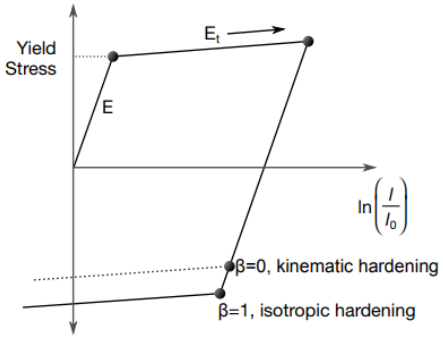

Figure 4.4: Material Model corrugated membrane as implemented. Difference between kinematic- and isotropic hardening is displayed

Table 4.4: gridsize and timestep input

gridsize	$3mm$
timestep	$2 * 10^{-5}s$

system. Strong coupling is coupling where iteratively the fluid- and structure are solved until their updates are satisfying the tolerance that set on beforehand.

Boundary conditions

The complete two dimensional model has a constraint in z-direction. The corrugated membrane is connected at the edges to the plywood. The plywood and foam, upper and lower edges are constraint except in x-direction. The right hand side of the foam is complete constrain in any direction.

Integration method

As discussed in chapter two, two time integration methods are available for the structural solver. Explicit and implicit. Explicit solvers are faster, but require a small time step. For

the model that is used here, an implicit time integration method is used. It is chosen for this integration method, because this allows the solver to complete solve the left and right hand side of the equation for FSI calculations. This results in a strong coupled system, which gives the best results.

For finding converging values the structural solver uses iterations, aiming for a minimal error. The convergence tolerance is based on a convergence on displacement OR energy. Both tolerances are set to a value of 10^{-8}.

Contact modelling

The corrugated membrane and the plywood are not attached to each other, but modelled using contact elements. For this a static friction coefficient should be applied. This is the friction force between the two layers. The value of this friction coefficient can lay between 0, no friction and 1 which is a full friction factor. For the simulations performed here, a friction factor of 0.18 is applied. These values are obtained from [25] in which a dry case of wood and steel friction is used.

4.1.3. Fluid-structure interaction input

The coupling method that is applied for the model is a strong two-way coupled system. In the next chapter the coupling method is tested. The FSI sensitive part in the construction is the corrugated membrane.

4.2. Verification

Results that are obtained from simulations will be verified in this section. Two methods are applied to compare the fluid behavior. 1) Contour analysis, 2) Particle Image Velocimetry.

4.2.1. Contour analysis

For verifying the fluid behaviour, the results of the simulation are compared to the experimental results. To obtain comparable material, contour analysis is performed. In which the contour lines between water and air are obtained based on color difference. The idea is to gray scale the image, then the boundaries are identified by taking the lines between light and dark colored areas. Python's module OpenCV [10] is used for this analysis.

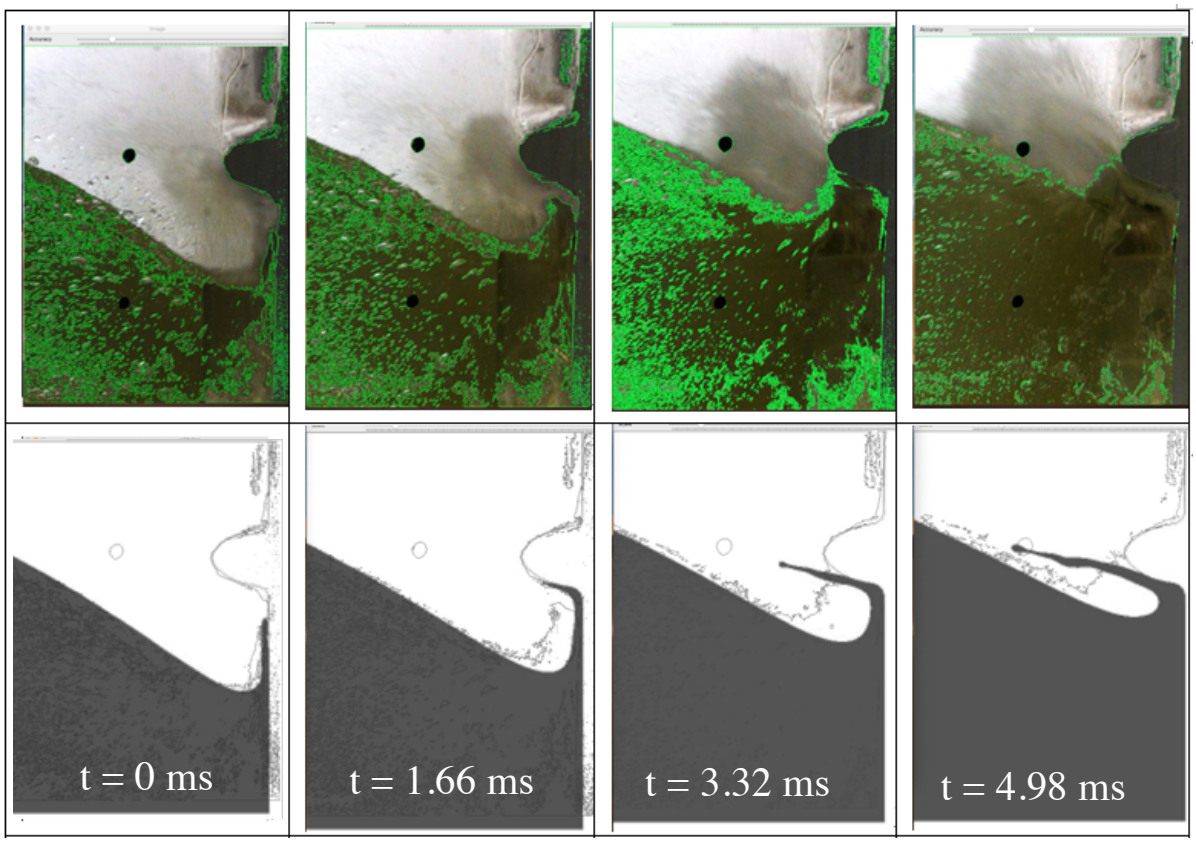

Figure 4.5: Upper 4 frames show experiment snapshots with highlighted the contour between water and air. Lower 4 frames show the CFD simulation with the same contour lines plotted.

Figure 4.5 shows that a large part of the fluid has a overlapping contour line, the area at the jet location shows less overlapping behaviour. The white spray that is visible in the experiments is not calculated in simulations. Also the shape of the jet, is different. This means that the first impacts on the corrugations that could be measured in experiments (i.e. force on the corrugation) is likely to show different results at this stage. Due to the general good results for the remainder of the fluid, the pressure peaks that are measured in experiments promise comparable results.

4.2.2. Particle Image velocimtery

Additional to the contour analysis of previous section, the behaviour below the fluid surface is considered using Particle Image Velocimtery (PIV). PIV is a technique that uses pixel differences between frames of a video to evaluate a motion. Due to the clear color differences between the fluid and air/spray, this technique can be applied on these frames. Vectors in Figure 4.6 are obtained containing direction and magnitude of the velocity. The work is based on [4]. In green the velocity stream lines of the simulation are plotted.

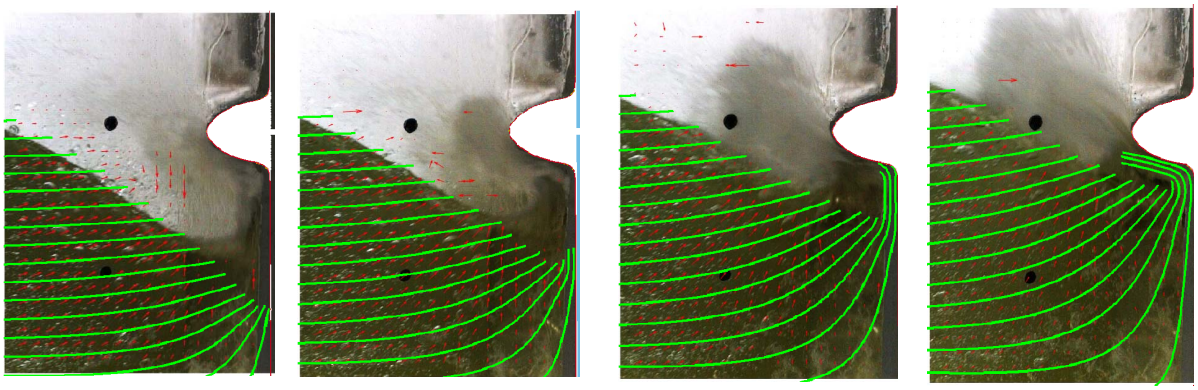

τ_1 τ_3 τ_5 τ_7

Figure 4.6: Experiment snapshot with Particle Image Velocimetry results (red –>) and simulation stream lines (– green). Timestep = 1.66ms

The observation leads to a slightly more horizontal velocities in the simulation, compared to the PIV results. Also, for the first frames that overlap the largest part of the simulation very well, it can be observed that the formation of the jet takes place later in the simulation. Interesting to see is that the last frames, where the fluid is being enclosed, show much better comparable results. This means that pressures along the vertical wall will take place later, but is is expected that the peak, at the enclosing of the fluid show similar behaviour.

4.3. Summary and conclusions

In this chapter the imput parameters for the fluid and structural model are discussed. The model is validated on fluid behavior and the following conclusions could be drawn:

- iCFD is an adequate technique to simulate the pressures for the local wave impact. Pressures are converged and compared to experimental data and is within a range of +/- 10%.
- For the fluid behaviour, the wave could be simulated with comparable results for the wave before impact. After impact, the major part of the wave was simulated well, the forming of the jet (ELP2) shows less overlapping results.

5

Analysis

In this chapter, an analysis on load an response is described for the Fluid-Structure Interaction model that is described in previous chapter. As starting point of the analysis, a wave impact similar to SLOSHEL experiments [8] is subjected to the structure at section 5.1. Then a case with higher impact velocities is described in 5.2. An addition of two more impacts is described in 5.3 and a brief analysis on a 3D rigid model is performed in 5.4.

5.1. Local Wave impact 7 m/s

In this section, the wave impact at 7 m/s is analysed. First, the behaviour of the fluid is analysed, followed by the structural behaviour in the order foam, plywood, membrane.

Four stages of local wave impact are distinguished. Elementary Loading Processes (ELP) such as they are applied in [8] are referred to. ELP1 refers to direct impact, see chapter 2.

1. Initial impact (ELP1)
2. Lower corrugation impact (ELP1)
3. Upper corrugation impact (ELP1)
4. Free vibration

5.1.1. Fluid behaviour

At three locations, pressures on the wall are measured during the simulation. These locations correspond to locations where high pressures are identified. For all locations, two cases are considered: a rigid (uncoupled)- and flexible (coupled) structure. In the fluid behaviour only the first three stages are considered, see Figure 5.1.

The first pressure peak is measured at initial impact (τ_1) and has values of 4.3 bar. The impact on the vertical wall causes the fluid to create jets along the wall (ELP2). The jets have a velocity that is approximately 25 m/s and reach the corrugations first at the lower corrugation (τ_2) and then at the upper corrugation (τ_3). The pressure near the lower corrugation (middle graph) is calculated at 2 bar. The pressure near the upper corrugation is 4.5 bar. An

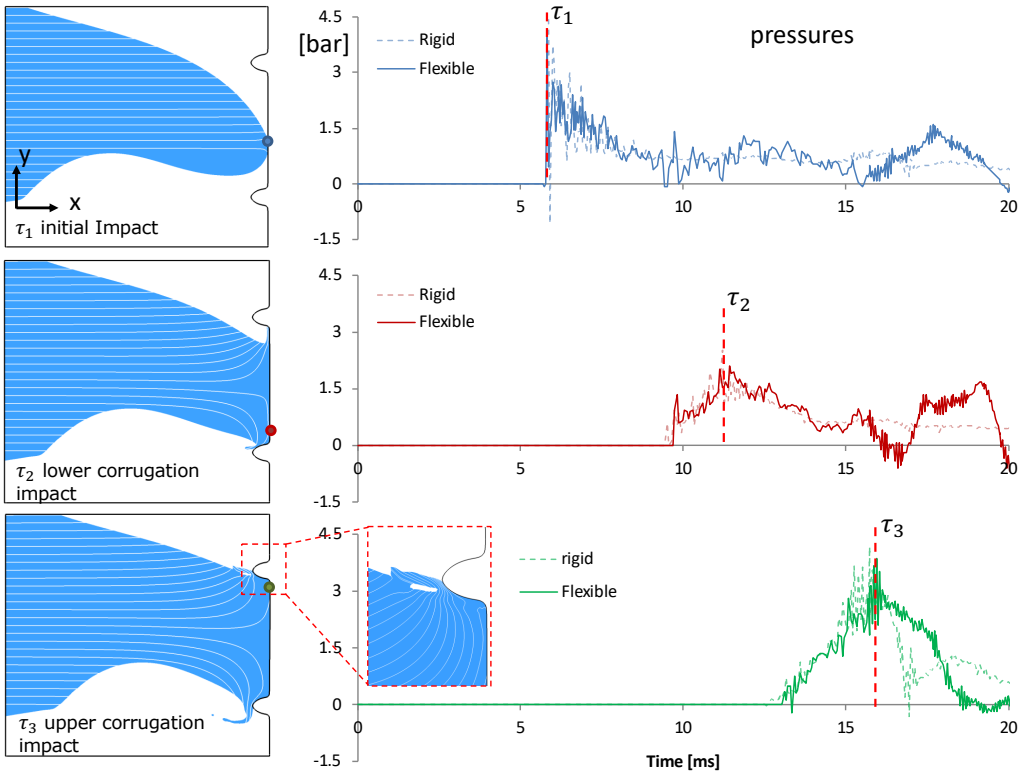

Figure 5.1: Fluid behaviour (left 3 figures) and fluid pressures (right) at three locations. Three stages have been identified (τ_i) Time between (peaks) $\tau_2 - \tau_1 = 5.6$ ms, $\tau_3 - \tau_2 = 4.5$ ms

enclosing behaviour takes place at the upper corrugation. The jet has changed direction and the remaining fluid volume still has its initial velocity, the two fluid streams are locked in the corner of the upper corrugation (see the close up at τ_3). This causes the third and highest pressure peak.

At the initial impact the results of coupled and uncoupled pressures overlap good, where the pressures after τ_3 are more constant compared to the coupled pressures. The vibration structure affect the pressures measured at the surface of the structure.

5.1.2. Structural response: Foam

In the displacement of the foam, four stages could be identified. In Figure 5.2 these stages are shown with dashed vertical lines. The pressures and responses are shown at four locations for coupled and uncoupled simulations.

The first stage is the initial impact. Here the foam bends at the location of impact. The highest displacement is found to be 0.9 mm at this stage. The second stage is the impact on the lower corrugation. The load is induced by the jet that is enclosed by the remainder of the fluid. The displacement of the foam is found to be 0.7mm. The third loading stage is on the upper corrugation. The displacement of the foam is found to be 1.2 mm. This is the maximum deflection that is measured in the foam according to this load case. In the fourth stage the the pressures are lower.

A clear change in pressure can be observed in at stage 4. Pressures in a coupled system tend

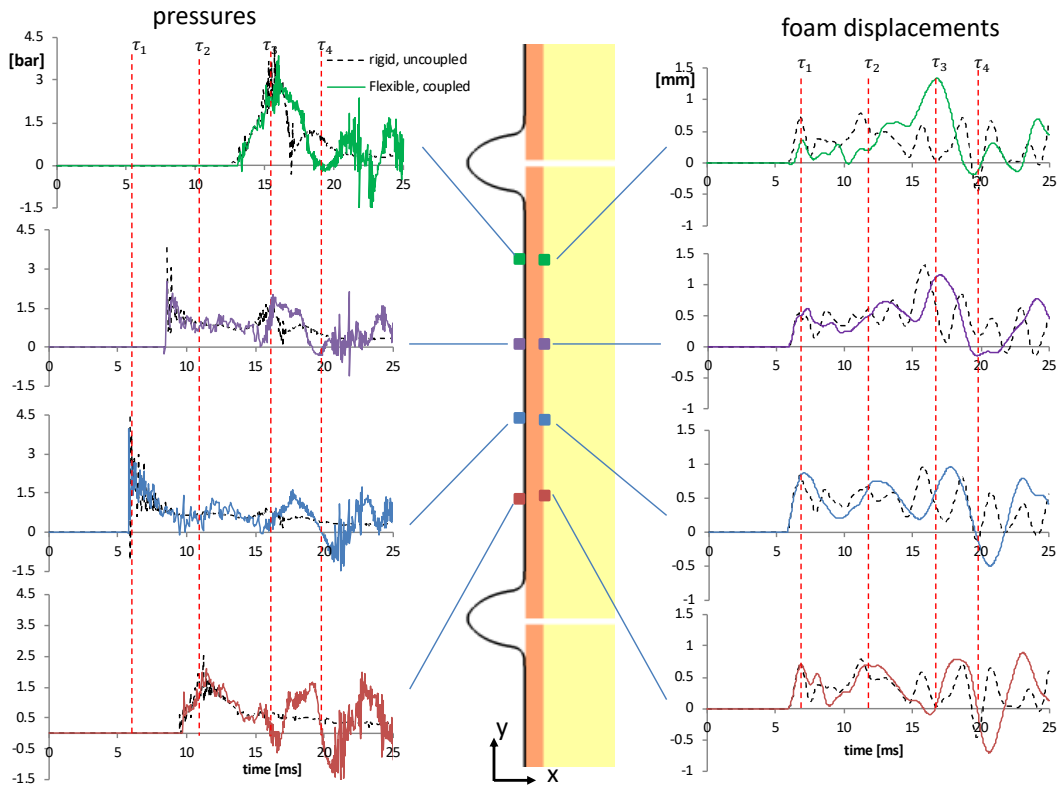

Figure 5.2: Fluid pressures on the membrane (left) and foam displacement (right) at four locations. Wet frequencies obtained with FFT frequencies of the foam displacement for time 0-25ms from top to bottom: 223Hz, 224Hz, 268Hz, 268Hz, dry frequencies 446Hz, 446Hz, 448Hz, 447Hz.

to follow the the motions of the beam. At stage 4, the corrugation-plywood-foam combination starts to vibrate wet mode for the coupled system and in a dry mode for a uncoupled system.

Coupled versus uncoupled displacements vary in amplitude and period. A Fast Fourier Transformation has been performed on the complete domain of the four time series of displacements, to analyse the spectral behaviour. The dry frequencies are in the order of magnitude as is found in a analytic model [9]. Dry frequencies are in the range of 446 and 448 Hz, wet frequencies are in the range of 223 and 268 Hz.

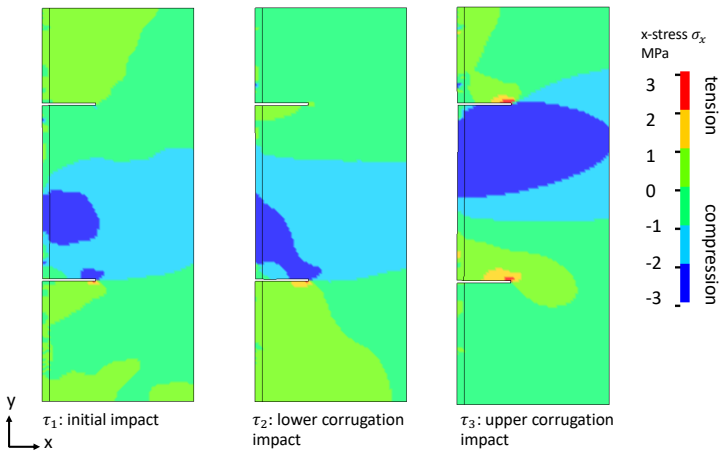

Figure 5.3: stresses in x-direction σ_x for the three stages

The stresses that have been measured (in x-direction σ_x) are shown in Figure 5.3. The enclosing of the fluid, stage 2 and 3 contains high stresses within the foam near the relaxation groove. The highest stresses within the foam are found in stage 3: enclosing the jet. The highest stresses that have been calculated for this impact wave correspond to 640 kPa in tension and 1.21 MPa in compression.

5.1.3. Structural response: Plywood

In the following part, a more detailed analysis is described of the plywood on the four stages that have been identified. Time frames are taken 0.4 ms before τ_i with $i = 1, 2, 3$, at τ_i and 0.4 ms after τ_i.

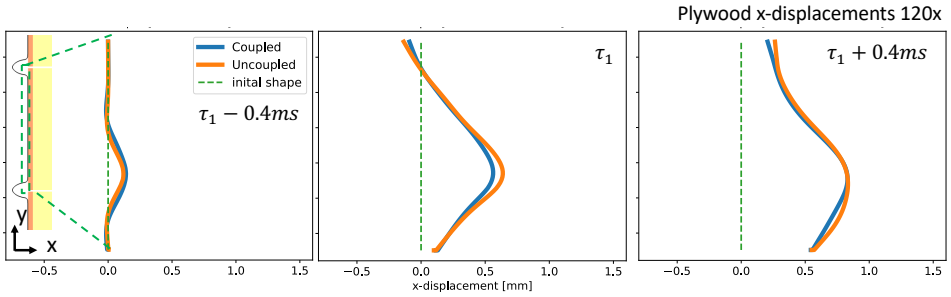

Figure 5.4: Deformed shapes of the plywood for τ_1. Coupled, Uncoupled simulations and initial shape.

In stage 1, local bending is observed at the area of impact see Figure 5.4. Also a heave motion is identified in positive x-direction. And, a pitch angle is identified that is counter clockwise. Differences between coupled and uncoupled motions are not too obvious in this stage.

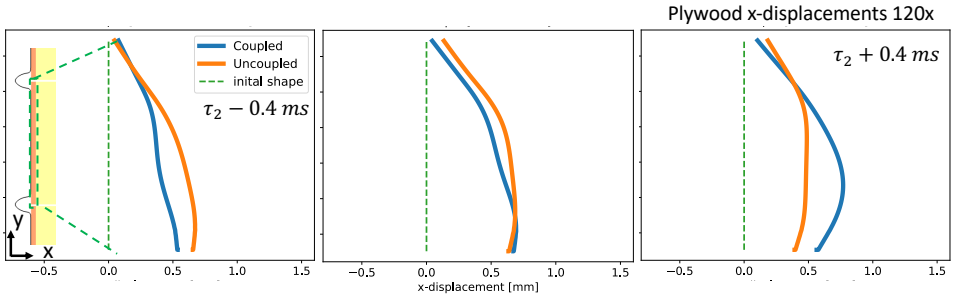

Figure 5.5: Deformed shapes of the plywood for τ_2. Coupled, Uncoupled simulations and initial shape.

Between stage 1 and stage 2, the forces are spread out on a larger area and the initial deformations of stage 1 spring-back slightly, mainly in heave motion.

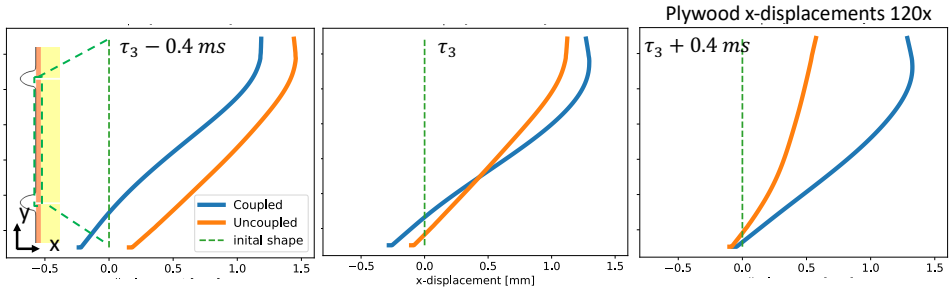

Figure 5.6: Deformed shapes of the plywood for τ_3. Coupled, Uncoupled simulations and initial shape.

At stage 2, the impact on the lower corrugation increases the pitch angle that was already induced in stage 1, in counterclockwise direction (Figure 5.5). In this stage also the heave

motion is increased. For the uncoupled analysis, the displacements in the foam are slightly higher.

At stage 3, the plywood is loaded similar but at the upper corrugation. This induces a pitch motion in opposite direction (Figure 5.6). The uncoupled motions start with larger deformations, but at $\tau_3 + 0.4ms$ the coupled responses are higher.

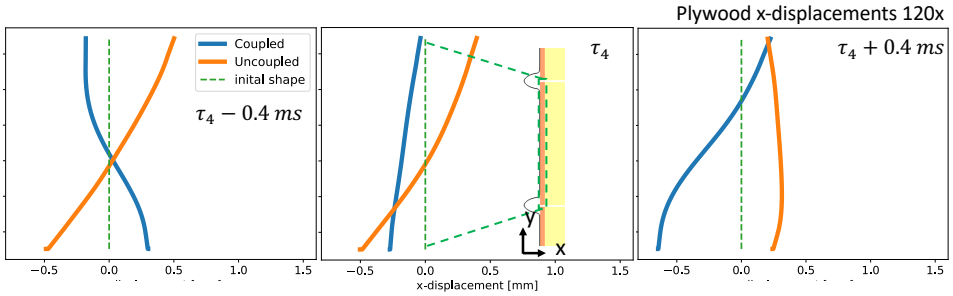

Figure 5.7: Deformed shapes of the plywood for τ_4. Coupled, Uncoupled simulations and initial shape.

After the high pressure peaks that were identified as stage 1-3, free-wet vibrations excites. This is descried in stage 4. In this stage less local bending takes part, but pitch and heave vibrations continue to take place. A clear pitch vibration can be found in Figure 5.7.

5.1.4. Structural response: corrugation

Drag forces have been measured in vertical direction. At maximum drag force measurement, the stresses are measured in the corrugations and shown in Figure 5.8. Outputs of the simulation were in a unit length of 1m and are divided by 3 so that they correspond to the distance between two corrugation knots. This analysis is only performed for the coupled simulation.

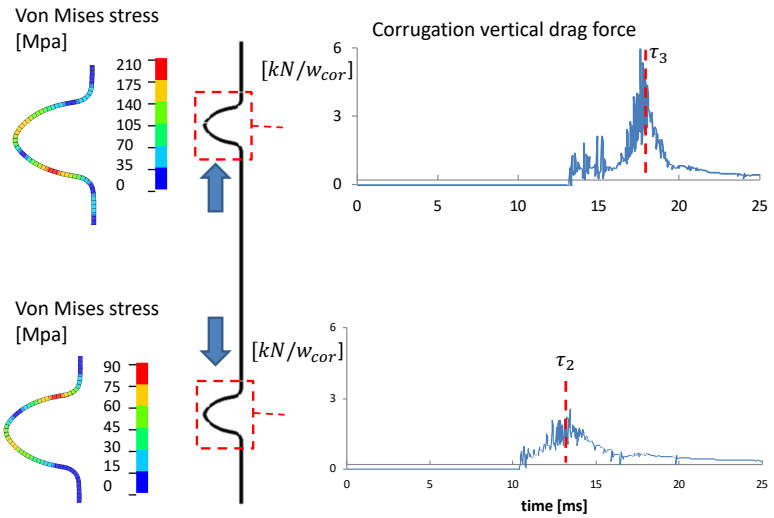

Figure 5.8: Corrugation (Von Mises) stress at its peak (left) and vertical drag force on the corrugtions (right). w_{cor} = $0.3m$

The force peaks intersect with the stages 2 and 3 that are identified earlier. The peaks that are calculated are 5.5 kN for the upper corrugation and 2.7 kN for the lower corrugation.

The stresses in the corrugation along the inner edges of the corrugations (see the red zone in Figure 5.8). The highest stresses are found at the on edged where jet interaction takes place and at the bend top of the corrugation just on the outer side of impact. The highest stress that have been measured is 181 MPa, where the yield stress is defined at 240 MPa. This means that no plastic behaviour in the corrugation takes place at this impact velocity.

The interaction behaviour that can be identified at the enclosing of the fluid is the following: first pressures result in a displacement of the foam, then the corrugation deforms on its long edge.

5.2. Impact velocity 16 m/s

In the case of a wave impacting at a velocity of 7 m/s, no plastic strain was measured within the corrugation. But, it was identified at one experimental case that plastic strain within the corrugation are a result of high pressures. Therefore the impact velocity of the initial simulation is increased. In this part, the structural response of the corrugation of a wave impacting with a velocity of 16 m/s is described.

Fluid behaviour

The fluid behaviour of this impact is, similar to lower velocities, divided into three stages in which the impact is high: τ_1: initial impact, τ_2: lower corrugation impact and stage 3 (τ_3): upper corrugation impact.

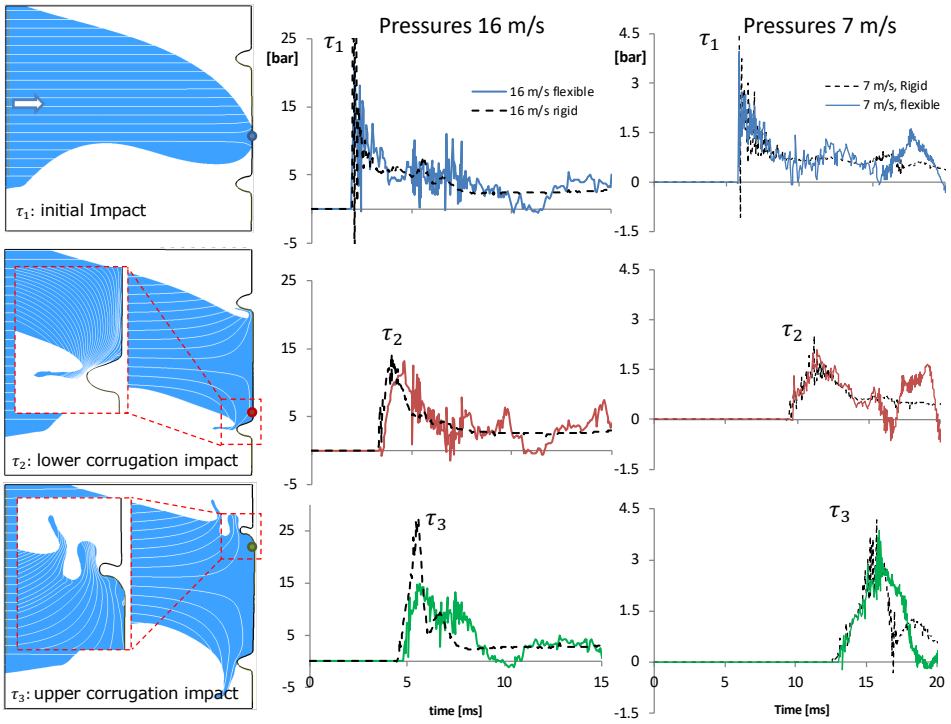

Figure 5.9: Fluid behaviour at 16 m/s impact wave. $\tau_2 - \tau_1 = 2.4ms$ and $\tau_3 - \tau_2 = 1.0ms$.

The pressures peaks of these different stages are 21, 13, 15 bar for stage 1,2,3. Additional

to this impact is the interaction due to the displacement of the inner edge of the upper corrugation. The edge is significantly deformed, elastic and plastic.

An interesting peak is found at the bottom middle figure. Here the pressure at τ_3 is significant higher than the coupled motion. This is the result of the deforming corrugation, which reduces the pressure.

structural response: foam and plywood

The foam displacement of the 16 m/s impact wave, Figure 1.7a (left) to the analyzed wave that impacts at 7 m/s (right). Four locations are considered.

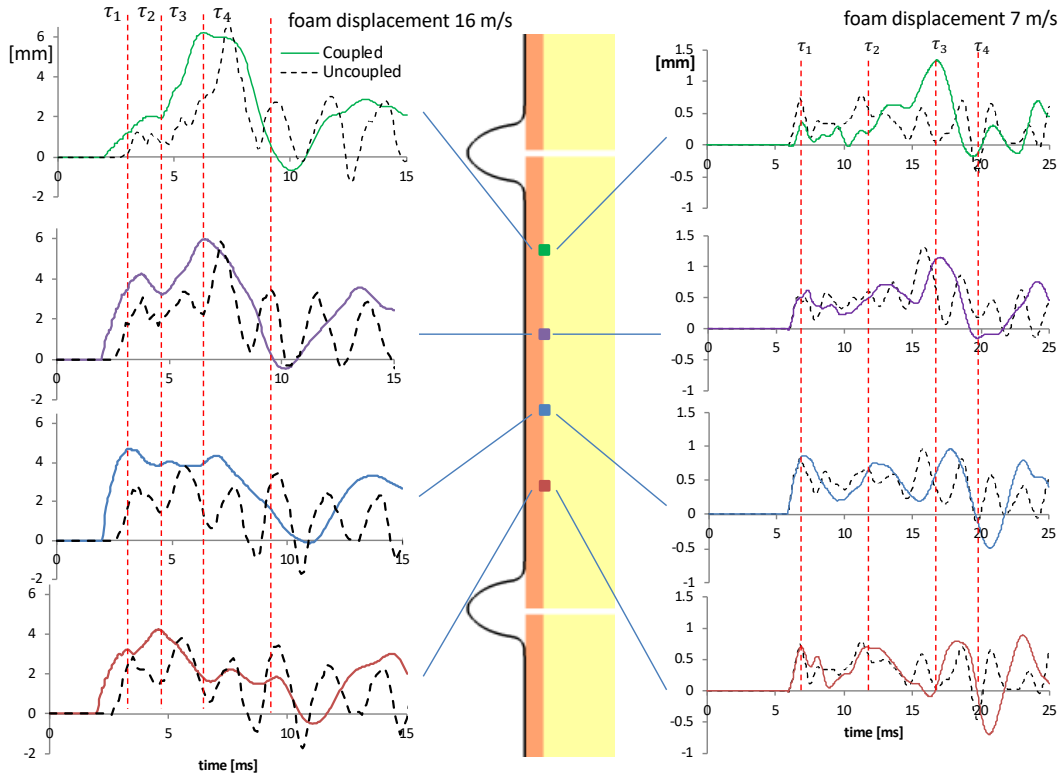

Figure 5.10: foam displacement 16 m/s. Foam response peaks: $\tau_2 - \tau_1 = 1.4ms$ and $\tau_3 - \tau_2 = 1.7ms$

Due to the high initial impact the complete foam part between the two relaxation grooves, is displaced. This results in the corrugations that bend slightly towards each other. Another behaviour that takes place is that the last peak displacement in the foam, at stage 3, is longer compared to the the displacement peak measured at lower velocities. This effect is assumed to be the effect of the deformation of the corrugation and therefore longer stagnating the fluid, leading to a longer pressure peak. Note that this effect does not take place in the uncoupled simulation.

structural response: corrugation

Then the impact on the corrugations itself it higher and the enclosing of the fluid causes a large deformation in the corrugation. This deformations causes stresses, that exceed yield stress limits of 240 MPa, which induces plastic stain.

In Figure 5.11 the displacements of 4 moments in time are shown for the upper corrugation (left). In the middle figure the stresses are shown at the moment of peak stress that was close to τ_3. On the right hand side plastic strain at the end of the simulation is shown.

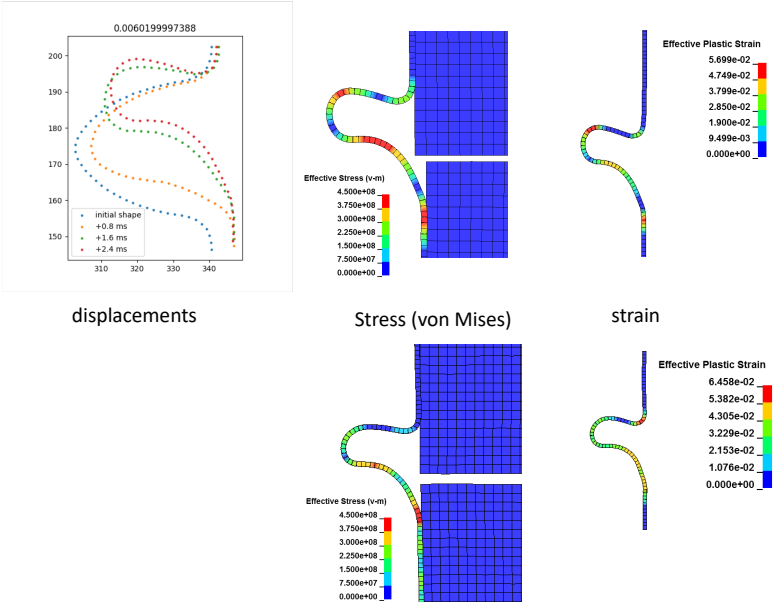

Figure 5.11: Corrugation response for an impact wave of 16 m/s. Top three graphs are coupled, the bottom graphs are uncoupled responses.

For this higher load case, the moment of plastic behaviour is found to be first initiated due to the jets that impact the corrugation, then the plastic strain is enlarged due to the enclosing of the fluid. The plastic deformation was found to be result of the pressures at stage 2 and stage 3.

Considering the corrugation response, the highest stresses that are calculated in the corrugation for the uncoupled simulation were 190 MPa, for the coupled simulation the highest stresses that were calculated were 181 MPa. Thus for this case the stresses in the uncoupled simulation are conservative.

Zooming in on these differences the plastic behaviour of the corrugation, this is influenced by the coupling method. The corrugated membrane and the foam have different vibration frequencies and modal shapes due to their change in geometry and material properties. In the coupled calculations, the vibrations of the corrugated membrane and the foam are controlled by the fluid impact. This induces the membrane and the plywood-foam layer to vibrate in the same frequency, leaving a minimal space between the corrugation and the foam. But, when considering the uncoupled system, and after the third impact stage, the membrane and foam start to vibrate at their own frequencies. This causes impact forces between the plywood and the corrugation. These impact forces induce additional plastic strain and different deformation shapes of the corrugations. These impact forces increase with increasing the impact velocity as can be read in the next section. But, because plastic behaviour starts to initiate at higher velocities, this statement is made only for impact velocities higher than 10 m/s.

5.3. Velocity variation

In this section the velocity of the impact is varied. Runs on different velocities are performed. 5, 7, 10, 15 and 16 m/s. To compare the model behaviour, impact pressure, foam- and plywood displacement, corrugation stress and -strain are compared. All values are based on local maximum values that are measured during the simulation. These local maximums are identified at the stages 1, 2 and 3.

At first maximum pressures are plotted at three locations Figure 5.12 (left three graphs) and the maximum foam displacements are plotted at the same locations (right three graphs).

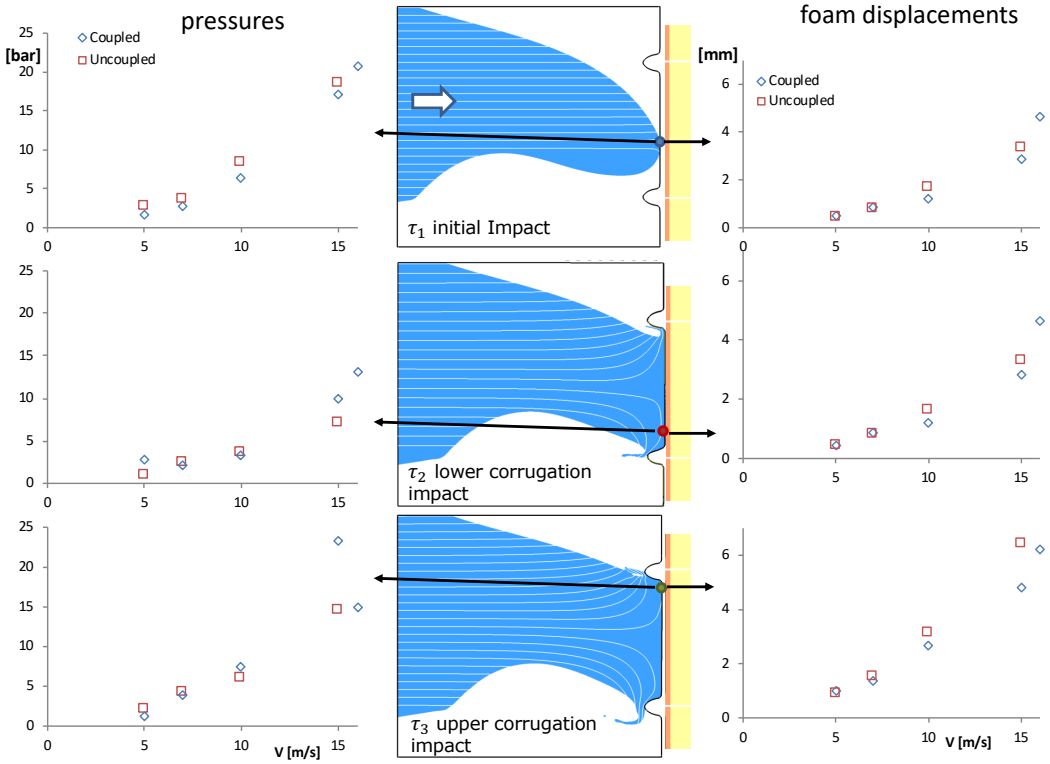

Figure 5.12: Fluid pressures (left) for 3 locations versus impact velocities. Displacements in the foam (right) versus impact velocities. Coupled and uncoupled simulations are considered.

At the initial impact pressures (top graphs in Figure 5.12) coupled pressures show for all velocities to have lower pressures. This was expected due to the fact that relative impact velocities are lower for for coupled simulations. A less expected result is found in the fact that near the corrugations, the pressures for coupled simulation show slightly higher pressures near corrugation, see Figure 5.12 (middle and bottom left graphs) at 15 m/s. This might be the effect of a too large time step, thus missing information. Another assumption is that local bending within the corrugation, changes the geometry and bend the corrugation inward, towards each other. This influences the fluid behaviour and increases the bending-off angle for the jets, which influences stage 2 and stage 3 of the enclosing of the fluid. In this study only a gird and time convergence study has been performed for the initial case. To testify the hypothesis, it is recommended to perform a convergence study on higher impact velocities.

For the structure response, Figure 5.12 (right hand side graphs), uncoupled simulations show fairly larger displacements compared to coupled simulation. This effect becomes more significant with increasing impact velocities and starts at a velocity of 10 m/s. Highest dif-

ferences were measured near the corrugation where displacement for uncoupled systems are 60% higher for the lower corrugation and 40 % higher for the upper corrugation. Thus for higher impact velocities, higher displacements are measured. These higher deformation has a significant effect on the displacement results. Displacements for uncoupled simulations are conservative.

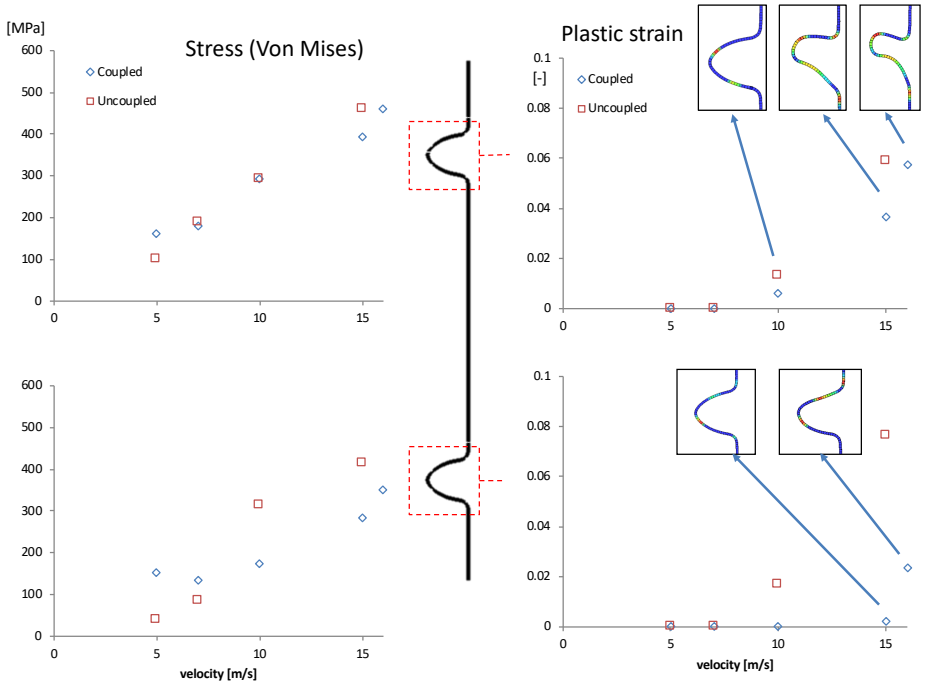

Figure 5.13: Von Mises stress versus impact velocity (left) and Plastic Strain ε versus impact velocity (right). Coupled and uncoupled simulations are considered

From the stress curve a linear behaviour can be observed in the maximum stresses that are calculated in the corrugated membrane, see Figure 5.13. For measuring these stresses and strains, the absolute maximums are used, in which the upper and the lower corrugation are distinguished. The stress curves show a linear behaviour. In which the majority of the simulations in uncoupled simulations is higher than in the coupled simulation. The largest differences are found with an impact velocity of 15 m/s. In this case, values of Von Mises stress for uncoupling are 10 % higher for the upper corrugation and 50 % higher for the lower corrugation.

Considering the plastic strain; the first simulation that shows plastic strain behaviour is found to be at 10 m/s. Two locations of the plastic deformation on the inner edge of the and on the outer edge of the upper corrugation see Figure 5.13. When impact velocities are higher and deformations also are, plastic strain locations start to occur at the corner points of the corrugations. Plastic deformations have not exceeded ultimate limit state for this impact velocities. The second phase of this graph is the increase in impact velocity after 10 m/s than plastic strain initiates, i.e. Von Mises stress exceeds yield criterion which is set at 240 MPa. At an impact velocity of 15 m/s, one-way coupled simulations show higher plastic strain: 60% higher for the upper corrugation, and $\varepsilon = 0.075$ compared to $\varepsilon = 0.001$ for a two-way coupled simulation on the lower corrugation.

5.4. 3D models

At last a 3D model is used to analyse the effects the 3D structure that is subjected to a 2D wave. The impact velocity for this wave is set at 7 m/s. The model consists of 4 knots in the corrugated membrane.

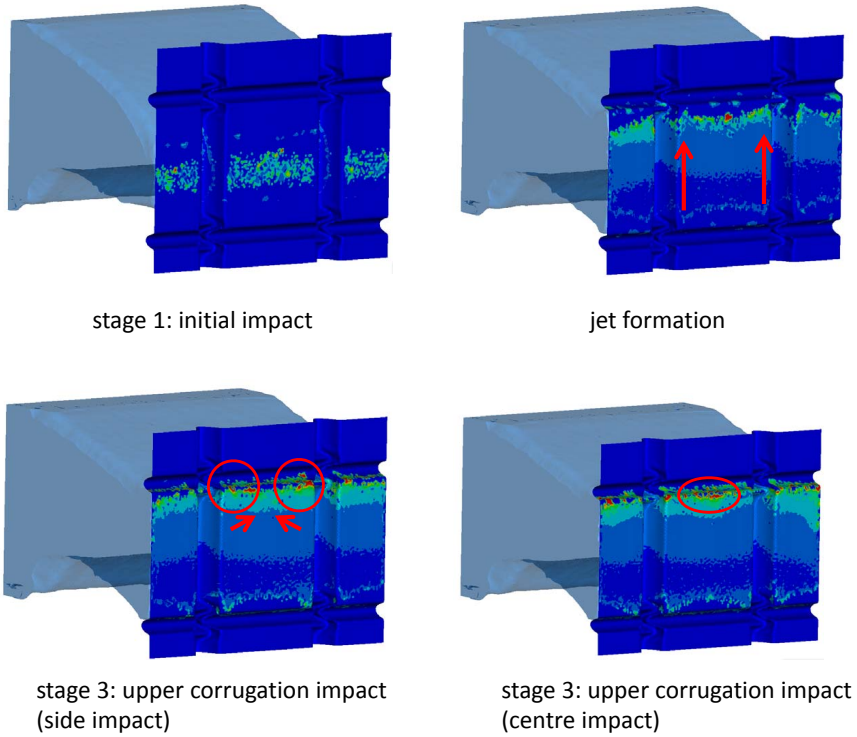

Figure 5.14: Pressures on a 3D model in in stage 1, jet formation (between stage 1 and 2) and stage 3: impact at the horizontal corrugation. Fluid velocities near the vertical corrugations are higher than in the vertical axis of symmetry. Therefore 3D effects take place

It was found here is an effect of filling up along the horizontal corrugations from the sides of the corrugations. The vertical corrugations slightly affect the fluid behaviour of the impacting wave. Near the vertical corrugations, accelerations of the fluid-jets are found to be higher than in the middle, see Figure 5.14 jet formation. The load process in stage 3 can now be divided into two parts: 1) the impact on the sides of the horizontal corrugation, near the knot area and the filling up of the remainder of the horizontal corrugation by the jet created in the middle AND the jets moving in from the sides. Therefore the effect of enclosing of the fluid at the middle of the horizontal corrugation, is enforced due to jets closing up the fluid from the side.

5.5. Summary and conclusions

A number of impact waves are subjected to a 2D mark III membrane. Velocities range from five- to sixteen meter per second. For the simulations. Uncoupled and coupled simulations are compared. From this a set of conclusions can be drawn.

Impact velocity 7 m/s

- Highest pressures are measured at stage 3 (τ_3) near the upper corrugation, at 4.5 bar. The jets that have been formed are enclosed by the wave and the corrugation, causing these high pressures. (Figure 5.1
- Peaks of pressure for coupled and uncoupled simulations are similar, but after the impact (τ_4) pressures of coupled systems starts to resonate, where uncoupled pressures keep stable. (Figure 5.1
- For uncoupled simulations only dry frequencies are found in a range of 446-448 Hz for the foam. For coupled simulations wet frequencies are found at 223-268 Hz. Figure 5.2.
- Foam response has three stress peaks calculated in the simulation. The highest peak is formed at stage 3, upper corrugation impact. The stresses are measured in x-direction and at a maximum 1.21 MPa in compression.
- The corrugations in the membrane show stress hot spots on the inner edges. At the upper corrugation the highest Von Mises stresses are calculated and are 210 MPa. For this impact wave plastic deformation was calculated.

Impact velocity 16 m/s

- For the higher load case at 16 m/s, the highest impact is calculated at the initial impact, stage 1, representing 18 bar, stage 3 represents 14 bar. Deformation of the corrugation causes the pressure near the corrugation bot be in the order of 2 lower for the coupled system.
- Foam responses in stage 3 are calculated at 5.5mm. Coupled systems are able to calculate wet frequencies, while in uncoupled systems only dry frequencies are obtained.
- Significant displacements are measured in the corrugations, resulting in high Von Mises stresses. Maximums are found to be 450 MPa in the upper corrugation. In this case buckling including plastic strain is calculated.

Multiple impact velocities

- Pressures are increasing with velocities. Pressure has shown to be a very sensible parameter showing often spiky behaviour.
- Deformation in the foam increases linear with increasing the impact velocity. For all displacements the uncoupled simulations show off higher displacements in the order of 10-25 %. Uncoupled simulations are therefore conservative.
- for corrugation response, uncoupled systems show higher values for stress with increasing when increasing the velocity. Stress is a sensible parameter. Plastic deformation shows of significant differences between coupled and uncoupled systems. Analysis on the 15 m/s shows that plastic strain show 120 % higher values for the unloaded loaded case. Uncoupled simulations are very conservative.

3D analysis

- A 3-Dimensional effect has been observed in the rigid corrugation model. Fluid flows near the vertical corrugations tend to have higher velocities, therefore hitting the horizontal corrugation first. These jets close up the fluid at the horizontal corrugation from

the side towards the middle, this results in slightly higher pressures than the 2D case. And is recommended to investigate further.

6

Conclusion

In this study, benchmarks were performed in chapter 3 to test appropriateness of several numerical methods. Besides, a benchmark was performed in order to quantify correct input parameters for the model with the following conclusions:

- Simulation results of the free surface of a Finite Element-Method-based incompressible Computational Fluid Dynamics (iCFD) method and Smoothed Particle Hydrodynamics (SPH) lay in between the results of a repeatable dam break experiment, in the range of +/- 2%. Both techniques are valid for simulating a free flow phenomena.
- Pressures on the wall of a dam break experiment with rigid wall for SPH has a spiky behaviour in the output signal. The standard deviation of SPH is twice as high as iCFD. Validating SPH results to experiments, will be less accurate.
- In 2D analysis, beam elements show a good balance between accurate results (<0.5% static and <1.6% dynamic compared to analytical results) CPU calculation time. For thicker structures, such as the foam and plywood, solid elements are required.

An application of the method was performed, by simulating an experimental wave-through impact between two corrugations. Results and conclusions that were found in this study

- Pressures of an impacting wave were compared to experimental results, from which was found that pressures of the simulating do not resonate such as were measured in experiments. Pressures were in the range of +/- 20 % and were often higher due to the incompressible property. The iCFD method is conservative in the sense that it computes often higher pressures.
- The free surface and below free surface of the global flow domain of the fluid was in good accordance to Particle Image Velocimerty and Contour Analysis results. The jet forming area (ELP2) shows less overlapping behaviour. The jet is faster and thinner. Pressures of global fluid behaviour can be used for analysis, but local jet impacts will not show similar pressures than was measured in experiments.

The analysis on this work has been performed on a wave-through impact, starting with velocities as they were performed in experiments. Thereafter, impact velocities have been increased so that plastic strain was simulated. Results and conclusions of this analysis were:

- The highest pressures of the local wave impact are measured near the upper corrugation was measured at a value 4.5 bar (τ_3). This is the result of the jet that is enclosed at high velocity by the global fluid domain and the corrugation.
- For lower impact velocities (5 and 7 m/s) the pressure peaks that were identified are similar for coupled and uncoupled simulations. When velocities increase, results between pressure peaks differ significant. With an impact velocity of 16 m/s the difference in peaks near the upper corrugation is 100%. This was the result of deformation of the corrugations. For the lower impact velocities, uncoupled simulations sulfide. For higher impact velocities, when large deformations occur, coupled simulations have more accurate pressures.
- Uncoupled simulations deliver dry frequencies that lay on 446-448 Hz. Coupled simulations simulate wet frequencies to be in the range of 223-268 Hz. For analysing the dynamics of the structure due to impact, only coupled systems provide reliable results.
- The maximum displacement in the foam was found at near the upper corrugation at 1.3 mm at the highest simulated impact velocity the displacement of the foam was calculated at 5.5 mm. Displacement in the foam increase linear with impact velocity at the velocity range 5 to 16 m/s. Amplitude of uncoupled simulations are slightly higher. Uncoupled simulations at higher velocities are conservative.
- Von Mises stresses that were measured in the corrugation had a maximum of 181 MPa for an impact velocity of 7 m/s. For higher impact velocities the Von Mises stress exceeds the yield stress criterion of 240MPa. And induces plastic strain. At higher impact velocities the uncoupled
- Plastic deformation has significant changes between coupled and uncoupled simulations. Uncoupled simulations have up to 120 % higher plastic strain values. For estimating plastic behaviour in the corrugated membrane, uncoupled simulations are inaccurate.
- Three dimensional effects were observed using a rigid structure. In this case local higher pressures were observed. It was observed that the jet velocities near the vertical corrugations are higher, therefore faster reaching the horizontal corrugation. Besides an enclosing behaviour upward, the jets near the vertical corrugations enclose toward the middle of the horizontal corrugation, causing higher pressures at the middle of the horizontal corrugation.

Coupled Fluid-Strucutre Interaction becomes beneficial when deformations within the structure become non-linear. For this specific case, when yield stress of the corrugations in the membrane is exceeded id est when plastic strain occurs, uncoupled simulations are not able to obtain accurate predictions for structural response.

7

Recommendations

On case of 3D analysis was performed in this work, and higher local pressures were found to be result of the 3D geometry of the corrugated membrane. It would be contributing and beneficial to investigate the responses on a full coupled 3D analysis. Input parameters from this thesis could be used, where beam elements for the membrane should be shell elements. Foam and Plywood could be modelled with solid elements.

The validity of the structural model is limited. The accuracy of structural response results leaves improvement. This could be done for example with making a connection with a analytical models, such as [9]. Experimental work can be used such as [23].

The conclusions that could be made on this study were specific, because one impact case was performed. The method that is described in chapter 4 could be used to perform analysis on different wave shapes, impact locations and velocities.

The number of conclusions that could be performed on higher impact velocities was limited, for example pressures results were spiky and coarse. Time step scaling for models at higher velocities should be performed.

Particle Image Velocimetry for initial velocities should be performed. Now the assumption was made that the fluid is moving with a velocity of approximately 7 m/s in purely horizontal direction. It is unlikely that the wave is a uniform propagating velocity field.

A

Reynolds number & Boundary layers

At the boundary of a structure two flow domains are distinguished by Ludwig Prantl. The domain inside the boundary layer and the domain outside the boundary layer, which is often defined as an area where 99% of the free flow velocity is achieved. Inside the boundary layer, the flow is strongly influenced by viscous forces. At high Reynolds numbers, where inertia forces dominate viscous forces, it is desirable to have a laminar boundary layer. In the wave impact, velocities, thus inertia forces are high. Therefore a boundary layer that is expected in a no-slip condition is not likely to develop in this short time window. Therefore, free-slip conditions are chose at all walls.

$$Re = \frac{\rho u L}{\mu} \tag{A.1}$$

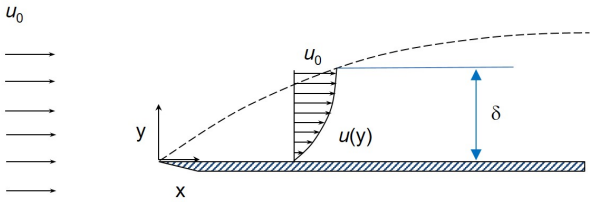

Figure A.1: Boundary layer thickness

The thickness squared of the boundary layer is proportional to the viscosity and time step of the fluid. The time step that is considered here is the wetting time of the area between the two corrugations.

$$\delta \sim \sqrt{\nu t} \tag{A.2}$$

This shows that for a small time interval the boundary layer is very small. The thickness over length is proportional to the the inverse of the square root of the Reynolds number

$$\frac{\delta}{x} \sim \sqrt{\frac{\nu}{xu(y)}} = \sqrt{\frac{1}{Re}} = \frac{1}{\sqrt{Re}} \tag{A.3}$$

Thus for a large Reynolds number the boundary layer required a large time distance to develop, which is not present between two corrugations. So it is assumed that no boundary layer develops.

B

Structural benchmark

Type	Element Size	Time Step	Frequency [Hz]	Difference	Deflection [m]	Difference
Beam 1	0.1	0.01	2.65	3.7%	0.022	2.3%
Beam 1	0.01	0.0005	2.802522463	1.8%		
Beam 1	0.1	0.001	2.805049282	1.9%	0.024289176	13.0%
Beam 1	0.025	0.01	2.647657841	3.8%	0.021605521	0.5%
Beam 1	0.0125	0.01	2.647657841	3.8%	0.021529841	0.1%
Beam 1	0.0125	0.005	2.825428923	2.6%		
Beam 1	0.0125	0.001	2.805049088	1.9%	0.0208	3.3%
Beam 2	0.025	0.01	2.647657841	3.8%	0.021610717	0.5%
Beam 2	0.025	0.005	2.851323829	3.6%		
Beam 7	0.1		2.04	25.9%	0.02178	1.3%
Beam 7	0.025		2.647657841	3.8%	0.019408018	9.7%
Shell quadratic	0.0025	0.01	2.58	6.3%	0.0227	5.6%
Shell quadratic	0.00125	0.01	2.794	1.5%		
Shell triangular	0.0025	0.01	2.781	1.0%	0.0193	10.2%
Shell triangular	0.0025	0.001	2.794	1.5%		
Solid 1		0.01	2.6476579	3.8%	0.02485421	15.6%
Solid 2		0.01	2.851323893	3.6%		

Bibliography

[1] 2015 world lng report. Technical report, International gas union, 2015.

[2] 2018 world lng report. Technical report, International gas union, 2018.

[3] Abacus. Abacus documentation version 6.5. https://classes.engineering.wustl.edu/2009/spring/mase5513/abaqus/docs/v6.5/books/gss/default.htm?startat=ch04s01.html, 2004. Accessed: 2019-1-17.

[4] Ronald J. Adrian and Jerry Westerweel. *Particle Image Velocimetry*. Cambridge University Press, 2011.

[5] AIAA. *Guide for the Verification and Validation of Computational Fluid Dynamics Simulations*. AIAA G-077-1998, 1998.

[6] G. K. Batchelor. *An introduction to Fluid Dynamics*. Cambebridge University press, The Edinburgh Building, Cambridge CB2 2RU, UK, 1967. ISBN 0521663962.

[7] Yuri Bazilevs, Kenji Takizawa, and Tayfun E. Tezduyar. *Computational Fluid-Structure Interaction*. Wiley, 2013.

[8] Hannes Bogaert. *An experimental investigation of sloshing impact physics in membrane LNG tanks on foating structures*. PhD thesis, Delft University of Technology, the Netherlands, 2018.

[9] R.W. Bos, J. H. den Besten, and M.L. Kaminski. Stress estimates for an lng cargo containment system. submitted work, 2019.

[10] G. Bradski. The OpenCV Library. *Dr. Dobb's Journal of Software Tools*, 2000.

[11] L.M.E. Bronswijk. Fluid-Structure Interaction of Self-Adaptive Marine Propellers. Master's thesis, TU Delft, the Netherlands, 2017.

[12] L. Brosset, W. Lafeber, H Bogaert, M. Marhem, P. Carden, and J. Maguire. A mark iii panel subjected to a flip-through wave impact: results from the sloshel project. In *The Twenty-first International Offshore and Polar Engineering Conference*, 2011.

[13] Inaki Caldichoury and Rodrigo R. Paz. Incompressible fluid solver in ls-dyna. Technical report, LS Dyna, 2014.

[14] R. Courant, H. Lewy, and K. Friedrichs. Über die partiellen differenzengleichungen der mathematischen physik. *Mathematische Annalen*, 1928.

[15] LS Dyna. Hourglass, 2018. URL https://www.dynasupport.com/howtos/element/hourglass.

[16] L. Eca and M. Hoekstra. On the influence of hte iteative error in the numerical uncertainty of ship viscous flow calculations. *Symposium on Naval Hydrodynamics*, 2006.

[17] Eric Gervaise, Pierr-Emmanel de Seze, and Stephane Maillard. Reliability-based methodology for sloshing assessment of membrane lng vessels. *International Journal of Offshore and Polar Engineering*, 19, 2009.

[18] M.L. Kaminski H. Bogaert, L. Brosset. Interaction between wave impacts and corrugations of markiii containment system for lng carriers: findings from the sloshel project. In *The Twentieth International Offshore and Polar Engineering Conference*, 2010.

[19] Nancy Hall. Navier-stokes equations. https://www.grc.nasa.gov/www/k-12/airplane/nseqs.html, 2015. Accessed: 2019-1-14.

[20] John O. Hallquist. *LS-Dyna Theory Manual*. Livermore Software Technology Corporation, 7374 Las Positas Road, Livermore, Calefornia 94551, 2006.

[21] H. K. Jeong and Y. S. Yang. Strength analysis of mark iii cargo containment system using anisotropic failure criteria. *Journal of Advanced Research in Ocean Engineering*, 1:211–226, 2015.

[22] M.L. Kaminski and Hannes Bogaert. Full scale sloshing impact tests. *The International Society of Offshore and Polar Engineers*, 38, 2009.

[23] Byung Chul Kim, Soon Ho Yoon, and Dai Gil Lee. Pressure resistance of the corrugated stainless steel membranes of lng. *Ocean Engineering*, 38, 2010.

[24] Peter Kopas, Milan Sága, Vladislav Baniari, Milan Vaško, and Marian Handrik. A plastic strain and stress analysis of bending and torsion fatigue specimens in the low-cycle fatigue region using the finite element methods. *Procedia Engineering*, 177:526–531, 12 2017. doi: 10.1016/j.proeng.2017.02.256.

[25] Radek Koubek and Karolina Dedicova. Friction of wood on steel, 2014.

[26] J. C. Martin and W. J. Moyce. An experimental study of the collapse of liquid columns on a rigid horizontal plane. Technical report, Royal Society, 1952.

[27] J. J. Monaghan. Smoothed particle hydrodynamics. *Astro. Astrophys*, 30, 1992.

[28] United Nations. Paris agreement. https://unfccc.int/process-and-meetings/the-paris-agreement/the-paris-agreement, 2015. Accessed: 2018-10-31.

[29] Intergovernmental Panel on Climate Change. Climate change 2014 summary for policymakers. http://ipcc.ch/pdf/assessment-report/ar5/syr/AR5_SYR_FINAL_SPM.pdf, 2014. Accessed: 2018-10-31.

[30] S. Osher and R. Fedkiw. *Level Set Methods and Dynamic Implicit Surfaces*. Springer, 2003.

[31] Y. Parihar, K. doshi, J. Saripilli, R. Joga, and S. dhavalikar. Strength assessment of membrane type contaainment system of lng carrier. *Proceedings of the International Offshore and Polar engineering Conference*, pages 1043–1050, 2016.

[32] D.H. Peregrine and L Thais. The effect of entrained air in violent water wave impacts. *Journal of Fluid Mechanics*, 1996.

[33] Jean-Herve Prevost. Plasticity theory for soil stress-strain behavior. *Journal of the Engineering Mechanics Division*, 104, 1978.

[34] John W. Slater. Uncertainty and error in cfd simulations. https://www.grc.nasa.gov/www/wind/valid/tutorial/errors.html, 2018. Accessed: 2018-10-22.

[35] FEM DATA STREAMLINER. Fem data streamliner shear locking. https://femds.com/FEM_Guidelines/Prevent_Shear_Locking, 2019. Accessed: 2019-1-17.

[36] Wing Kam Liu James M. Kennedy Ted Belytschko, Jame Shau-Jen Ong. Hourglass control in linear and nonlinear problems. *Computer Methods in Applied Mechanics and Engineering*, 43:251–276, 5 1984.

[37] unknown. Elements. https://www.dynasupport.com/tutorial/ls-dyna-users-guide/elements, 2019. Accessed: 2019-1-23.